

Analysis Procedures for Evaluating Superheavy Load Movement on Flexible Pavements, Volume VI: Appendix E, Ultimate and Service Limit Analyses

PUBLICATION NO. FHWA-HRT-18-054

OCTOBER 2019



U.S. Department of Transportation
Federal Highway Administration

Research, Development, and Technology
Turner-Fairbank Highway Research Center
6300 Georgetown Pike
McLean, VA 22101-2296

FOREWORD

The movement of superheavy loads (SHLs) on the Nation's highways is an increasingly common, vital economic necessity for many important industries, such as chemical, oil, electrical, and defense. Many superheavy components are extremely large and heavy (gross vehicle weights in excess of a few million pounds), and they often require specialized trailers and hauling units. At times, SHL vehicles have been assembled to suit the load being transported, and therefore, the axle configurations have not been standard or consistent. Accommodating SHL movements without undue damage to highway infrastructure requires the determination of whether the pavement is structurally adequate to sustain the SHL movement and protect any underground utilities. Such determination involves analyzing the likelihood of instantaneous or rapid load-induced shear failure of the pavement structure.

The goal of this project was to develop a comprehensive analysis process for evaluating SHL movement on flexible pavements. As part of this project, a comprehensive mechanistic-based analysis approach consisting of several analysis procedures was developed for flexible pavement structures and documented in a 10-volume series of Federal Highway Administration reports—a final report and 9 appendices.⁽¹⁻⁹⁾ This is *Analysis Procedures for Evaluating Superheavy Load Movement on Flexible Pavements, Volume VI: Appendix E, Ultimate and Service Limit Analyses*, which details the analysis procedures for investigating the risk of ultimate and localized shear failure under SHL-vehicle movements. A deflection-based service limit analysis for limiting the amount of pavement surface deflection under an SHL-vehicle is also presented. This report is intended for use by highway agency pavement engineers responsible for assessing the structural adequacy of pavements in the proposed route and identifying mitigation strategies, where warranted, in support of the agency's response to SHL-movement permit requests.

Cheryl Allen Richter, Ph.D., P.E.
Director, Office of Infrastructure
Research and Development

Notice

This document is disseminated under the sponsorship of the U.S. Department of Transportation (USDOT) in the interest of information exchange. The U.S. Government assumes no liability for the use of the information contained in this document.

The U.S. Government does not endorse products or manufacturers. Trademarks or manufacturers' names appear in this report only because they are considered essential to the objective of the document.

Quality Assurance Statement

The Federal Highway Administration (FHWA) provides high-quality information to serve Government, industry, and the public in a manner that promotes public understanding. Standards and policies are used to ensure and maximize the quality, objectivity, utility, and integrity of its information. FHWA periodically reviews quality issues and adjusts its programs and processes to ensure continuous quality improvement.

TECHNICAL REPORT DOCUMENTATION PAGE

1. Report No. FHWA-HRT-18-054	2. Government Accession No.	3. Recipient's Catalog No.	
4. Title and Subtitle Analysis Procedures for Evaluating Superheavy Load Movement on Flexible Pavements, Volume VI: Appendix E, Ultimate and Service Limit Analyses		5. Report Date July 2019	
		6. Performing Organization Code	
7. Author(s) Hadi Nabizadeh (ORCID: 0000-0001-8215-1299), Mohamed Nimeri (ORCID: 0000-0002-3328-4367), Elie Y. Hajj (ORCID: 0000-0001-8568-6360), Raj V. Siddharthan (ORCID: 0000-0002-3847-7934), and Sherif Elfass (ORCID: 0000-0003-3401-6513)		8. Performing Organization Report No. WRSC-UNR-201710-01E	
9. Performing Organization Name and Address Department of Civil and Environmental Engineering University of Nevada 1664 North Virginia Street Reno, NV 89557		10. Work Unit No.	
		11. Contract or Grant No. DTFH61-13-C-00014	
12. Sponsoring Agency Name and Address Office of Infrastructure Research and Development Federal Highway Administration Turner-Fairbank Highway Research Center 6300 Georgetown Pike McLean, VA 22101		13. Type of Report and Period Covered Final Report; August 2013–July 2018	
		14. Sponsoring Agency Code HRDI-20	
15. Supplementary Notes Nadarajah Sivaneswaran (HRDI-20; ORCID: 0000-0003-0287-664X), Office of Infrastructure Research and Development, Turner-Fairbank Highway Research Center, served as the Contracting Officer's Representative.			
16. Abstract The movement of superheavy loads (SHLs) on the Nation's highways is an increasingly common, vital economic necessity for many important industries, such as chemical, oil, electrical, and defense. SHL hauling units are much larger in size and weight than standard trucks. SHL gross vehicle weights may be in excess of a few million pounds, so they often require specialized trailers and components with nonstandard spacing between tires and axles. Accommodating SHL-vehicle movements requires determining whether pavement is structurally adequate and analyzing the likelihood of instantaneous or rapid load-induced shear failure. In this study, as part of the Federal Highway Administration project, Analysis Procedures for Evaluating Superheavy Load Movement on Flexible Pavements, methods for conducting shear failure and service limit analyses in a flexible pavement under an SHL-vehicle movement were developed. Shear failure analysis involves an ultimate and localized analysis conducted to check the adequacy of a pavement structure to withstand shear failure. Meyerhof's general bearing capacity equation was adopted to investigate the possibility of ultimate shear failure, and the Drucker–Prager yield criterion was used to examine the likelihood of localized shear failure (yield). The service limit analysis was conducted using a deflection-based approach because excessive surface deflections resulting from SHL-vehicle movements may give rise to the rapid deterioration of a pavement structure and development of premature surface distresses (e.g., permanent deformation). To avoid rapid pavement deterioration, SHL vehicle-induced surface deflections were limited to a determined allowable surface deflection.			
17. Key Words Superheavy load, flexible pavement, ultimate shear failure, localized shear failure, service limit, falling weight deflectometer		18. Distribution Statement No restrictions. This document is available through the National Technical Information Service, Springfield, VA 22161. http://www.ntis.gov	
19. Security Classif. (of this report) Unclassified	20. Security Classif. (of this page) Unclassified	21. No. of Pages 42	22. Price N/A

SI* (MODERN METRIC) CONVERSION FACTORS

APPROXIMATE CONVERSIONS TO SI UNITS

Symbol	When You Know	Multiply By	To Find	Symbol
LENGTH				
in	inches	25.4	millimeters	mm
ft	feet	0.305	meters	m
yd	yards	0.914	meters	m
mi	miles	1.61	kilometers	km
AREA				
in ²	square inches	645.2	square millimeters	mm ²
ft ²	square feet	0.093	square meters	m ²
yd ²	square yard	0.836	square meters	m ²
ac	acres	0.405	hectares	ha
mi ²	square miles	2.59	square kilometers	km ²
VOLUME				
fl oz	fluid ounces	29.57	milliliters	mL
gal	gallons	3.785	liters	L
ft ³	cubic feet	0.028	cubic meters	m ³
yd ³	cubic yards	0.765	cubic meters	m ³
NOTE: volumes greater than 1000 L shall be shown in m ³				
MASS				
oz	ounces	28.35	grams	g
lb	pounds	0.454	kilograms	kg
T	short tons (2000 lb)	0.907	megagrams (or "metric ton")	Mg (or "t")
TEMPERATURE (exact degrees)				
°F	Fahrenheit	5 (F-32)/9 or (F-32)/1.8	Celsius	°C
ILLUMINATION				
fc	foot-candles	10.76	lux	lx
fl	foot-Lamberts	3.426	candela/m ²	cd/m ²
FORCE and PRESSURE or STRESS				
lbf	poundforce	4.45	newtons	N
lbf/in ²	poundforce per square inch	6.89	kilopascals	kPa
APPROXIMATE CONVERSIONS FROM SI UNITS				
Symbol	When You Know	Multiply By	To Find	Symbol
LENGTH				
mm	millimeters	0.039	inches	in
m	meters	3.28	feet	ft
m	meters	1.09	yards	yd
km	kilometers	0.621	miles	mi
AREA				
mm ²	square millimeters	0.0016	square inches	in ²
m ²	square meters	10.764	square feet	ft ²
m ²	square meters	1.195	square yards	yd ²
ha	hectares	2.47	acres	ac
km ²	square kilometers	0.386	square miles	mi ²
VOLUME				
mL	milliliters	0.034	fluid ounces	fl oz
L	liters	0.264	gallons	gal
m ³	cubic meters	35.314	cubic feet	ft ³
m ³	cubic meters	1.307	cubic yards	yd ³
MASS				
g	grams	0.035	ounces	oz
kg	kilograms	2.202	pounds	lb
Mg (or "t")	megagrams (or "metric ton")	1.103	short tons (2000 lb)	T
TEMPERATURE (exact degrees)				
°C	Celsius	1.8C+32	Fahrenheit	°F
ILLUMINATION				
lx	lux	0.0929	foot-candles	fc
cd/m ²	candela/m ²	0.2919	foot-Lamberts	fl
FORCE and PRESSURE or STRESS				
N	newtons	0.225	poundforce	lbf
kPa	kilopascals	0.145	poundforce per square inch	lbf/in ²

ANALYSIS PROCEDURES FOR EVALUATING SUPERHEAVY LOAD MOVEMENT ON FLEXIBLE PAVEMENTS PROJECT REPORT SERIES

This volume is the sixth of 10 volumes in this research report series. Volume I is the final report, and Volume II through Volume X consist of Appendix A through Appendix I. Any reference to a volume in this series will be referenced in the text as “Volume II: Appendix A,” “Volume III: Appendix B,” and so forth. The following list contains the volumes:

Volume	Title	Report Number
I	Analysis Procedures for Evaluating Superheavy Load Movement on Flexible Pavements, Volume I: Final Report	FHWA-HRT-18-049
II	Analysis Procedures for Evaluating Superheavy Load Movement on Flexible Pavements, Volume II: Appendix A, Experimental Program	FHWA-HRT-18-050
III	Analysis Procedures for Evaluating Superheavy Load Movement on Flexible Pavements, Volume III: Appendix B, Superheavy Load Configurations and Nucleus of Analysis Vehicle	FHWA-HRT-18-051
IV	Analysis Procedures for Evaluating Superheavy Load Movement on Flexible Pavements, Volume IV: Appendix C, Material Characterization for Superheavy Load Movement Analysis	FHWA-HRT-18-052
V	Analysis Procedures for Evaluating Superheavy Load Movement on Flexible Pavements, Volume V: Appendix D, Estimation of Subgrade Shear Strength Parameters Using Falling Weight Deflectometer	FHWA-HRT-18-053
VI	Analysis Procedures for Evaluating Superheavy Load Movement on Flexible Pavements, Volume VI: Appendix E, Ultimate and Service Limit Analyses	FHWA-HRT-18-054
VII	Analysis Procedures for Evaluating Superheavy Load Movement on Flexible Pavements, Volume VII: Appendix F, Failure Analysis of Sloped Pavement Shoulders	FHWA-HRT-18-055
VIII	Analysis Procedures for Evaluating Superheavy Load Movement on Flexible Pavements, Volume VIII: Appendix G, Risk Analysis of Buried Utilities Under Superheavy Load Vehicle Movements	FHWA-HRT-18-056
IX	Analysis Procedures for Evaluating Superheavy Load Movement on Flexible Pavements, Volume IX: Appendix H, Analysis of Cost Allocation Associated with Pavement Damage Under a Superheavy Load Vehicle Movement	FHWA-HRT-18-057
X	Analysis Procedures for Evaluating Superheavy Load Movement on Flexible Pavements, Volume X: Appendix I, Analysis Package for Superheavy Load Vehicle Movement on Flexible Pavement (SuperPACK)	FHWA-HRT-18-058

TABLE OF CONTENTS

CHAPTER 1. INTRODUCTION	1
CHAPTER 2. ULTIMATE FAILURE ANALYSIS	5
2.1. QU EQUATION.....	5
2.1.1. Bearing Capacity Factors	6
2.2. APPLICATION OF MEYERHOF'S QU EQUATION	8
2.3. SHL-VEHICLE CASES.....	10
2.3.1. 3D-Move Analysis Inputs	10
2.3.2. Determination of q_{ave}	14
2.3.3. Bearing Capacity Failure Analysis.....	15
2.4. BEARING CAPACITY ASSOCIATED WITH SLOPING SHOULDER.....	15
CHAPTER 3. SERVICE LIMIT ANALYSES.....	19
3.1. LOCALIZED SHEAR FAILURE ANALYSIS UNDER SHL-VEHICLE	
MOVEMENTS.....	19
3.2. DEFLECTION-BASED SERVICE LIMIT ANALYSIS UNDER SHL-VEHICLE	
MOVEMENTS.....	23
3.2.1. Determination of FWD_{equiv}	24
3.2.2. Determination of FWD_{allow}	25
CHAPTER 4. SUMMARY	27
REFERENCES.....	29

LIST OF FIGURES

Figure 1. Flowchart. Overall SHL-vehicle analysis methodology	2
Figure 2. Equation. Meyerhof's q_u	5
Figure 3. Equation. Calculation of Nq	6
Figure 4. Equation. Calculation of Nc	6
Figure 5. Equation. Calculation of $N\gamma$	6
Figure 6. Equation. Calculation of Fcs	6
Figure 7. Equation. Calculation of Fqs	6
Figure 8. Equation. Calculation of $F\gamma s$	6
Figure 9. Equation. Calculation of Fcd for $D_f/B \leq 1$ and $\phi = 0$	6
Figure 10. Equation. Calculation of Fqd for $D_f/B \leq 1$ and $\phi = 0$	6
Figure 11. Equation. Calculation of $F\gamma d$ for $D_f/B \leq 1$ and $\phi = 0$	6
Figure 12. Equation. Calculation of Fcd for $D_f/B \leq 1$ and $\phi > 0$	7
Figure 13. Equation. Calculation of Fqd for $D_f/B \leq 1$ and $\phi > 0$	7
Figure 14. Equation. Calculation of $F\gamma d$ for $D_f/B \leq 1$ and $\phi > 0$	7
Figure 15. Equation. Calculation of Fcd for $D_f/B > 1$ and $\phi = 0$	7
Figure 16. Equation. Calculation of Fqd for $D_f/B > 1$ and $\phi = 0$	7
Figure 17. Equation. Calculation of $F\gamma d$ for $D_f/B > 1$ and $\phi = 0$	7
Figure 18. Equation. Calculation of Fcd for $D_f/B > 1$ and $\phi > 0$	7
Figure 19. Equation. Calculation of Fqd for $D_f/B > 1$ and $\phi > 0$	7
Figure 20. Equation. Calculation of $F\gamma d$ for $D_f/B > 1$ and $\phi > 0$	7
Figure 21. Equation. Calculation of Fci	7
Figure 22. Equation. Calculation of Fyi	7
Figure 23. Illustration. Example configuration (LA-8T-14) of an LaDOTD-permitted SHL vehicle (continuous axle configuration).....	8
Figure 24. Illustration. Example configuration (LA-12T-16) of an LaDOTD-permitted SHL vehicle (fragmented axle configuration).....	9
Figure 25. Illustration. Example configuration of an NDOT-permitted SHL vehicle.....	9
Figure 26. Equation. Calculation of q_{ave}	10
Figure 27. Illustration. SHL-vehicle axle configuration (case No. 2: LA-8T-14) and nucleus of SHL configuration	12
Figure 28. Illustration. 3D schematic of the pavement structure in 3D-Move Analysis	13
Figure 29. Chart. 3D view of σ_v distribution on top of the SG with five axles with six tires each (SHL case No. 2: LA-8T-14, 100°F)	14
Figure 30. Chart. Top view of σ_v distribution on top of the SG with five axles with six tires each (SHL case No. 2: LA-8T-14, 100 °F)	14
Figure 31. Chart. 3D view of σ_v distribution at middle dual tires on top of the SG (SHL case No. 2: LA-8T-14, 100 °F).....	15
Figure 32. Chart. Bearing capacity failure under a rough rigid foundation on a slope	16
Figure 33. Equation. Calculation of ultimate bearing capacity for a shallow strip foundation.....	16
Figure 34. Illustration. Drucker–Prager and Mohr–Coulomb yield surfaces	19
Figure 35. Equation. Drucker–Prager yield criterion.....	20
Figure 36. Equation. Calculation of ζ	20
Figure 37. Equation. Calculation of κ	20

Figure 38. Equation. Calculation of q	20
Figure 39. Equation. Calculation of p	20
Figure 40. Chart. Representation of the Drucker–Prager yield criterion in the q – p plot.....	21
Figure 41. Equation. Calculation of FOS using the Drucker–Prager yield criterion.....	21
Figure 42. Equation. Calculation of FOS as a function of ζ and κ	21
Figure 43. Equation. Calculation of σ_{oct} using principal stresses	22
Figure 44. Equation. Calculation of τ_{oct} using principal stresses.....	22
Figure 45. Equation. Calculation of $p_{applied}$ using σ_{oct}	22
Figure 46. Equation. Calculation of $q_{applied}$ using τ_{oct}	22
Figure 47. Chart. FOS for the SHL-vehicle nucleus.....	23
Figure 48. Chart. FWD load–deflection curve.....	24
Figure 49. Equation. Calculation of SSR.....	25
Figure 50. Chart. Representation of τ_{max} and $\tau_{mobilized}$	25
Figure 51. Equation. Calculation of $\tau_{mobilized}$	25
Figure 52. Equation. Calculation of τ_{max}	25
Figure 53. Equation. Calculation of equivalent σ_d	26
Figure 54. Equation. Calculation of equivalent σ_c	26
Figure 55. Chart. FWD load–SSR curve	26

LIST OF TABLES

Table 1. Developed analysis procedures to evaluate SHL movement on flexible pavements	3
Table 2. Material properties of each layer	13
Table 3. E^* values for a typical dense-graded HMA with PG64-22	13
Table 4. Phase angle values for a typical dense-grade HMA with PG64-22.....	13
Table 5. N_c associated with a sloped shoulder	17
Table 6. N_q associated with a sloped shoulder	18
Table 7. N_γ associated with a sloped shoulder	18

LIST OF ABBREVIATIONS AND SYMBOLS

Abbreviations

3D	three-dimensional
AC	asphalt concrete
CAB	crushed aggregate base
<i>FOS</i>	factor of safety
FWD	falling weight deflectometer
GVW	gross vehicle weight
HMA	hot-mix asphalt
LaDOTD	Louisiana Department of Transportation and Development
NDOT	Nevada Department of Transportation
No.	number
PG	performance grade
SG	subgrade
SHL	superheavy load
SSR	shear stress ratio
SuperPACK	Superheavy Load Pavement Analysis PACKAge

Symbols

$A_{affected}$	affected area
b	distance from the edge of the slope
B	width (or diameter) of the foundation
c	cohesion
dx	differential of the variable x
dy	differential of the variable y
D_0	center deflection at the center of the falling weight deflectometer plate
D_f	depth of the foundation measured from the ground surface
E^*	dynamic modulus
F_{cd}	depth factor with respect to cohesion
F_{ci}	load inclination factor with respect to cohesion
F_{cs}	shape factor with respect to cohesion
F_{qd}	depth factor with respect to overburden
F_{qi}	load inclination factor with respect to overburden
F_{qs}	shape factor with respect to overburden
FWD_{allow}	allowable falling weight deflectometer load level
FWD_{equiv}	equivalent falling weight deflectometer load level
F_{yd}	depth factor with respect to unit weight
F_{yi}	load inclination factor with respect to unit weight
F_{ys}	shape factor with respect to unit weight
I_1	first invariant of the stress tensor
\bar{I}_{2D}	second invariant of the deviator stress tensor
l	foundation length
N_c	bearing capacity factor with respect to cohesion

Nq	bearing capacity factor with respect to overburden
$N\gamma$	bearing capacity factor with respect to unit weight
p	mean normal stress in Drucker–Prager yield criterion
$p_{applied}$	induced mean normal stress
q	deviator stress in Drucker–Prager yield criterion
\bar{q}	overburden pressure at the foundation level
$q_{applied}$	induced deviator stress
q_{ave}	average uniform vertical stress
$q_{failure}$	Drucker–Prager deviator stress at failure
q_u	general bearing capacity
V_0'	velocity of soil in the transition zone at point E on the side without slope
V_3	velocity of soil at the end of transition zone
V_3'	velocity of soil at the end of log spiral on the side without slope
V_p	velocity of foundation
β	inclination of the slope
β_i	vertical inclination of a load on a foundation
γ	unit weight of soil
δ_{SHL}	superheavy load vehicle–induced surface deflection
θ	logarithmic spiral angle
ζ	Drucker–Prager material constant associated with the angle of internal friction
κ	Drucker–Prager material constant associated with the angle of internal friction and cohesion
σ_1	major principal stress
σ_2	intermediate principal stress
σ_3	minor principal stress
σ_c	confining stress
σ_d	deviator stress
σ_{ij}	stress tensor
σ_{oct}	octahedral normal stress
σ_v	vertical stress
τ_{max}	maximum shear strength
τ_{oct}	octahedral shear stress
$\tau_{mobilized}$	applied (mobilized) shear stress
ϕ	angle of internal friction
ϕ_m	mobilized angle of internal friction

CHAPTER 1. INTRODUCTION

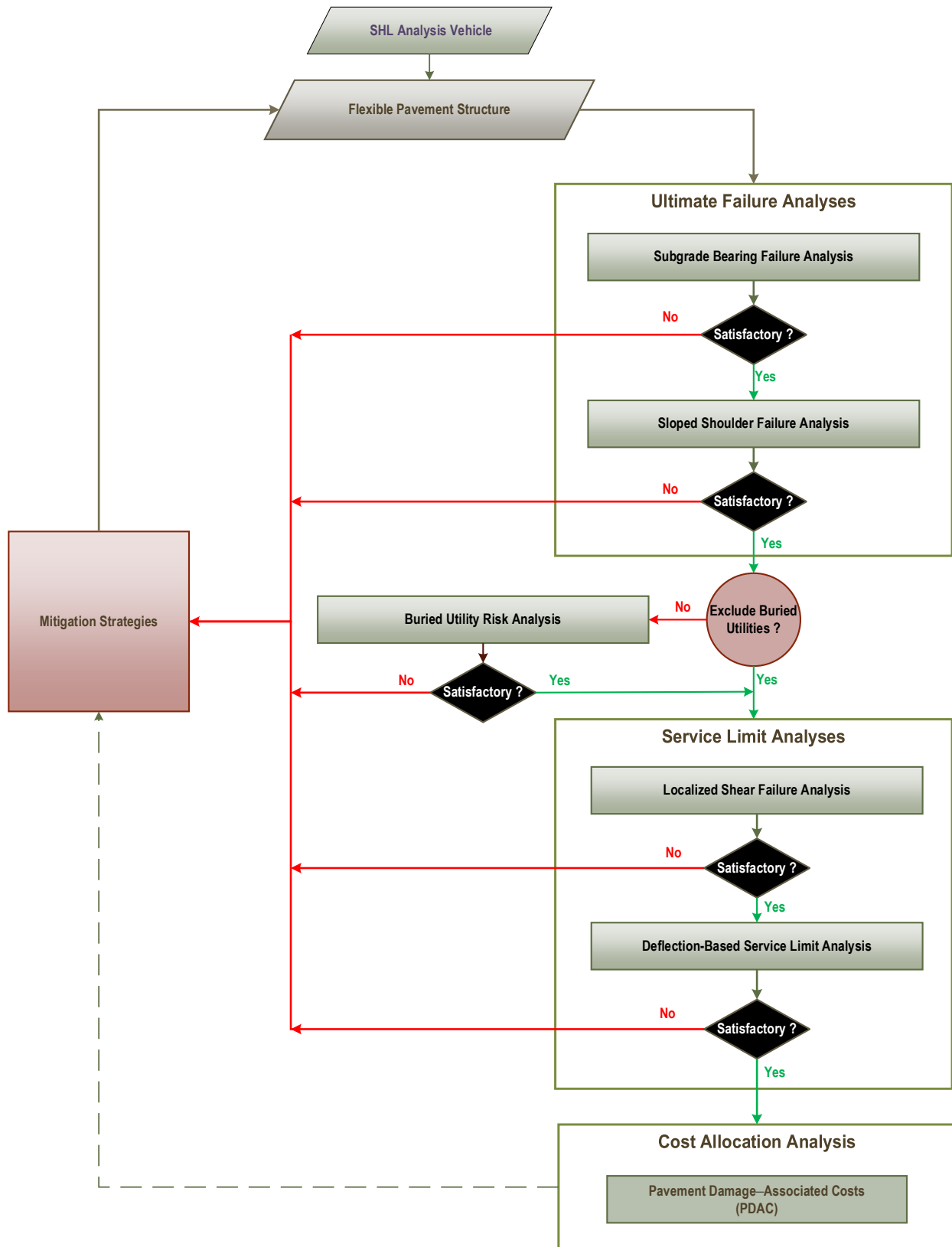
Many industries, such as chemical, oil, electrical, and defense, require the movement of superheavy loads (SHLs) on the Nation's highways. SHL hauling units are much larger in size and weight than standard trucks, often with gross vehicle weights (GVWs) in excess of a few million pounds. Accordingly, SHL vehicles frequently necessitate specialized trailers and components with nonstandard spacing between tires and axles. Accommodating SHL-vehicle movements requires determining whether a pavement is structurally adequate and analyzing the likelihood of instantaneous or rapid load-induced shear failure. Figure 1 shows the flowchart of the overall approach developed as part of this Federal Highway Administration project, Analysis Procedures for Evaluating Superheavy Load Movement on Flexible Pavements. In general, the approach consists of the following four major components:

- Ultimate failure analyses.
- Buried utility risk analysis.
- Service limit analyses.
- Cost allocation analysis.

Mitigation strategies may be needed at any stage of the evaluation process when the calculated results fail to meet the respective requirements imposed (e.g., when results indicate a high potential for shear failure of the pavement or damage to buried utilities).

As shown in figure 1, the first step of this approach involves a risk analysis of instantaneous or rapid load-induced ultimate shear failure. Subgrade (SG) is generally the weakest layer in a pavement structure. Thus, a bearing failure analysis should be performed to investigate the likelihood of general bearing capacity (q_u) failure under an SHL vehicle within the influenced zone of an SG layer. Sloped-shoulder failure analysis, which examines the bearing capacity failure and edge-slope stability associated with a sloped ground under an SHL-vehicle movement, would be the next step. If the ultimate failure analyses reveal no failure in the sloped shoulder, a buried utility risk analysis should be conducted (when applicable). In this analysis, induced stresses and deflections by an SHL vehicle on existing buried utilities are evaluated and compared to established design criteria. Subsequently, if no mitigation strategies are needed, service limit analyses for localized shear failure and deflection-based service limits should be conducted. A localized shear failure analysis is performed to investigate the possibility of failure at the critical location on top of an SG layer under an SHL vehicle. A deflection-based service limit analysis assesses the magnitude of load-induced pavement deflections during an SHL-vehicle movement. This analysis, for instance, may suggest the need for mitigation strategies to meet the imposed acceptable surface-deflection limits. After successfully completing all previously described analyses (i.e., ultimate failure analyses, buried utility risk analysis, and service limit analyses), a cost allocation analysis should be conducted.

A summary of the various analysis procedures developed in this study and the associated objectives (including related volume numbers) are summarized in table 1. This report (Volume VI: Appendix E) is the sixth of 10 volumes and presents the ultimate failure analyses and service limit analysis of a flexible pavement subjected to an SHL-vehicle movement.



© 2018 UNR.

Figure 1. Flowchart. Overall SHL-vehicle analysis methodology.

Table 1. Developed analysis procedures to evaluate SHL movement on flexible pavements.

Procedure	Objective
SHL analysis vehicle	Identify segment(s) of the SHL-vehicle configuration that can be regarded as representative of the entire SHL vehicle (Volume III: Appendix B) ⁽³⁾
Flexible pavement structure	Characterize representative material properties for existing pavement layers (Volume IV: Appendix C and Volume V: Appendix D) ^(4,5)
SG bearing failure analysis	Investigate instantaneous ultimate shear failure in pavement SG (Volume VI: Appendix E)
Sloped-shoulder failure analysis	Examine the stability of sloped pavement shoulder under SHL-vehicle movement (Volume VII: Appendix F) ⁽⁶⁾
Buried utility risk analysis	Perform risk analysis of existing buried utilities (Volume VIII: Appendix G) ⁽⁷⁾
Localized shear failure analysis	Inspect the likelihood of localized failure (yield) in the pavement SG (Volume VI: Appendix E)
Deflection-based service limit analysis	Investigate the development of premature surface distresses (Volume VI: Appendix E)
Cost allocation analysis	Determine pavement damage-associated cost attributable to SHL-vehicle movement (Volume IX: Appendix H) ⁽⁸⁾

The nonstandard heavy loading of an SHL-vehicle movement can render a critical condition (i.e., distress mode) of instantaneous ultimate shear failure, localized shear failure, or excessive deflection in a pavement surface. Meyerhof's q_u equation is an ideal method to examine the risk of instantaneous shear failure since it is a well-established and validated analysis procedure for foundation design under loading conditions of static or slow-moving vehicles. The distributed vertical stress (σ_v) induced by an SHL vehicle on top of an SG layer in comparison to the bearing capacity of the SG layer is used to identify the possibility of ultimate shear failure in a pavement structure. The ultimate failure analysis focuses on the SG layer as it is generally the weakest layer in a pavement structure. In cases of sloping ground, a modified bearing capacity approach is applied. Mitigation strategies might be necessary to prevent the risk of bearing capacity failure.

Once a bearing capacity investigation confirms a pavement structure can adequately withstand general shear failure, the possibility of localized shear failure needs to be evaluated. Such an analysis is conducted by computing the load-induced stress level on top of the SG layer. Any stress level higher than the SG failure criterion indicates a likelihood of localized failure (i.e., yield) and warrants the need for mitigation strategies. The Drucker–Prager yield criterion is used in this study to determine the SG failure criterion.

While ultimate and localized shear failure analyses are checks for failure condition, they do not provide any information regarding surface deflection under an SHL-vehicle movement. In other words, though shear failure analyses may reveal that a pavement structure is capable of sustaining an SHL-vehicle movement without experiencing any shear failure, excessive surface

deflections resulting from an SHL-vehicle loading can induce rapid deterioration of the pavement structure and development of premature surface distresses (e.g., permanent deformation). Therefore, induced surface deflection by an SHL-vehicle should be limited. Mitigation strategies might be required if this analysis, which is referred to as a deflection-based service limit analysis, reveals excessive load-induced surface deflections.

CHAPTER 2. ULTIMATE FAILURE ANALYSIS

In this study, the risk of instantaneous shear failure was investigated using Meyerhof's q_u theory. The distributed σ_v on top of an SG layer induced by an SHL vehicle in comparison to the bearing capacity of an SG layer was used to identify the possibility of ultimate shear failure in the pavement structure. Meyerhof's q_u equation can be applied to estimate the bearing capacity of an SG layer. This chapter presents Meyerhof's q_u theory and its application in relation to an SHL-vehicle movement.

2.1. q_u EQUATION

Soil has three failure modes: general, local, and punching shear failures. Terzaghi presented a comprehensive theory for evaluating q_u of shallow strip foundations using a uniform pressure to mimic the effect of soil above the bottom of the foundation.^(10,11) Several studies aiming to improve the estimation of q_u followed Terzaghi's work.⁽¹²⁻¹⁵⁾ Meyerhof suggested a more general form for q_u that accounts for continuous, rectangular, square, and circular foundations and any inclination in the load.⁽¹⁵⁾ Meyerhof's q_u equation is shown in figure 2. Section 2.1.1 describes the various components of Meyerhof's q_u equation.

$$q_u = (c)(Nc)(Fcs)(Fcd)(Fci) + (\bar{q})(Nq)(Fqs)(Fqd)(Fqi) + \left(\frac{1}{2}\gamma\right)(B)(N\gamma)(F\gamma s)(F\gamma d)(F\gamma i)$$

Figure 2. Equation. Meyerhof's q_u .

Where:

c = cohesion.

Nc = bearing capacity factor with respect to c .

Fcs = shape factor with respect to c .

Fcd = depth factor with respect to c .

Fci = load inclination factor with respect to c .

\bar{q} = overburden pressure at the foundation level.

Nq = bearing capacity factor with respect to overburden.

Fqs = shape factor with respect to overburden.

Fqd = depth factor with respect to overburden.

Fqi = load inclination factor with respect to overburden.

γ = unit weight of soil.

B = width (or diameter) of the foundation.

$N\gamma$ = bearing capacity factor with respect to unit weight.

$F\gamma s$ = shape factor with respect to unit weight.

$F\gamma d$ = depth factor with respect to unit weight.

$F\gamma i$ = load inclination factor with respect to unit weight.

2.1.1. Bearing Capacity Factors

Values of the bearing capacity factors— N_c (originally derived by Prandtl), N_q (presented by Reissner), and N_γ (presented by Caquot and Kerisel and Vesic)—for a given angle of internal friction (ϕ) can be determined using the equations presented in figure 3 through figure 5. (See references 11, 14, 16, and 18.)

$$N_q = \tan^2 \left(45 + \frac{\phi}{2} \right) e^{\pi \tan \phi}$$

Figure 3. Equation. Calculation of N_q .

$$N_c = (N_q - 1) \cot \phi$$

Figure 4. Equation. Calculation of N_c .

$$N_\gamma = 2 (N_q + 1) \tan \phi$$

Figure 5. Equation. Calculation of N_γ .

The equations to calculate F_{cs} , F_{qs} , and $F_{\gamma s}$ for a given ϕ , B , and foundation length (l) are presented in figure 6 through figure 8.

$$F_{cs} = 1 + \left(\frac{B}{l} \right) \left(\frac{N_q}{N_c} \right)$$

Figure 6. Equation. Calculation of F_{cs} .

$$F_{qs} = 1 + \left(\frac{B}{l} \right) \tan \phi$$

Figure 7. Equation. Calculation of F_{qs} .

$$F_{\gamma s} = 1 - 0.4 \left(\frac{B}{l} \right)$$

Figure 8. Equation. Calculation of $F_{\gamma s}$.

The equations to calculate F_{cd} , F_{qd} , and $F_{\gamma d}$ are presented in figure 9 through figure 20, where D_f is the depth of the foundation measured from the ground surface.

$$F_{cd} = 1 + 0.4 \left(\frac{D_f}{B} \right)$$

Figure 9. Equation. Calculation of F_{cd} for $D_f/B \leq 1$ and $\phi = 0$.

$$F_{qd} = 1$$

Figure 10. Equation. Calculation of F_{qd} for $D_f/B \leq 1$ and $\phi = 0$.

$$F_{\gamma d} = 1$$

Figure 11. Equation. Calculation of $F_{\gamma d}$ for $D_f/B \leq 1$ and $\phi = 0$.

$$Fcd = Fqd - \left(\frac{1 - Fqd}{Nc \tan\phi} \right)$$

Figure 12. Equation. Calculation of Fcd for $D_f/B \leq 1$ and $\phi > 0$.

$$Fcd = 1 + 2 \tan\phi (1 - \sin\phi)^2 \left(\frac{D_f}{B} \right)$$

Figure 13. Equation. Calculation of Fqd for $D_f/B \leq 1$ and $\phi > 0$.

$$F\gamma d = 1$$

Figure 14. Equation. Calculation of $F\gamma d$ for $D_f/B \leq 1$ and $\phi > 0$.

$$Fcd = 1 + 0.4 \tan^{-1} \left(\frac{D_f}{B} \right)$$

Figure 15. Equation. Calculation of Fcd for $D_f/B > 1$ and $\phi = 0$.

$$Fqd = 1$$

Figure 16. Equation. Calculation of Fqd for $D_f/B > 1$ and $\phi = 0$.

$$F\gamma d = 1$$

Figure 17. Equation. Calculation of $F\gamma d$ for $D_f/B > 1$ and $\phi = 0$.

$$Fcd = Fqd - \left(\frac{1 - Fqd}{Nc \tan\phi} \right)$$

Figure 18. Equation. Calculation of Fcd for $D_f/B > 1$ and $\phi > 0$.

$$Fqd = 1 + 2 \tan\phi (1 - \sin\phi)^2 \tan^{-1} \left(\frac{D_f}{B} \right)$$

Figure 19. Equation. Calculation of Fqd for $D_f/B > 1$ and $\phi > 0$.

$$F\gamma d = 1$$

Figure 20. Equation. Calculation of $F\gamma d$ for $D_f/B > 1$ and $\phi > 0$.

The equations to calculate Fci , Fqi , and $F\gamma i$ for a given vertical inclination of a load on a foundation (β_i) are expressed in figure 21 and figure 22.

$$Fci = Fqi = \left(1 - \frac{\beta_i}{90} \right)^2$$

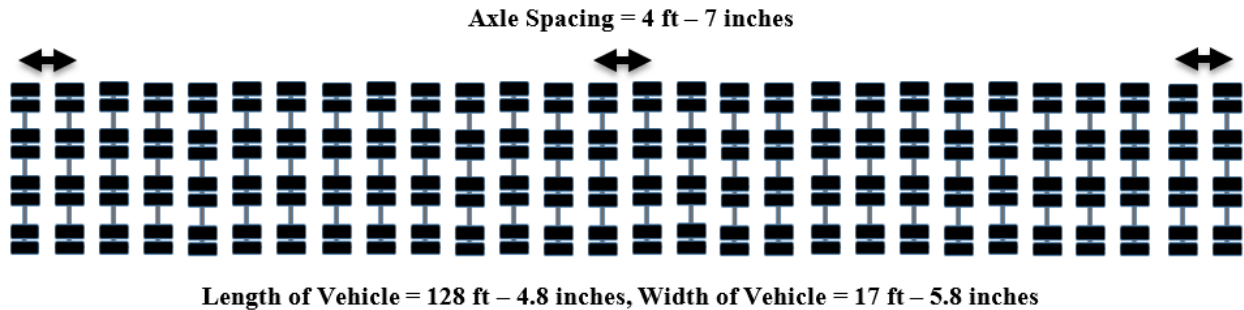
Figure 21. Equation. Calculation of Fci .

$$F\gamma i = \left(1 - \frac{\beta_i}{\phi} \right)^2$$

Figure 22. Equation. Calculation of $F\gamma i$.

2.2. APPLICATION OF MEYERHOF'S q_u EQUATION

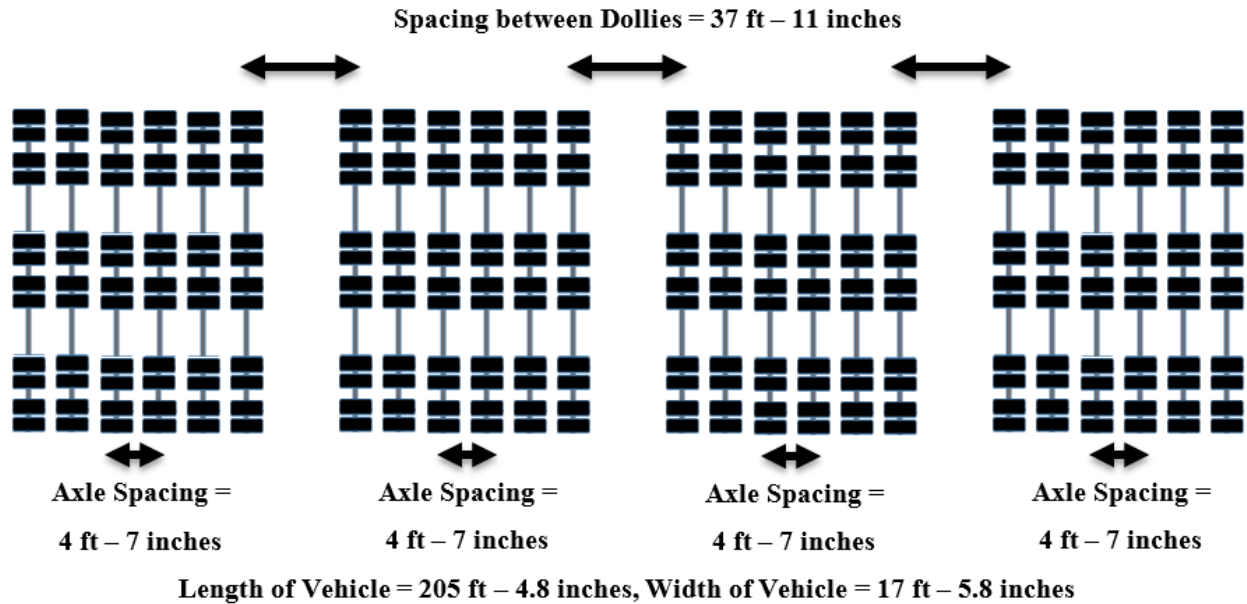
SHL vehicles typically vary in terms of axle and tire configurations (i.e., number of axles, spacing between the axles, number of tires per axle, spacing between the tires, and tire loads). In general, SHL vehicles fall into three categories. In the first category, similar axles (i.e., similar number of tires per axle, spacing between the tires, and tire loads) are evenly distributed along the length of an SHL vehicle. The spacing between axles is close enough that stress distributions from tires on two adjacent axles clearly overlap beyond a specific depth in the pavement (e.g., the top of the SG layer). The Louisiana Department of Transportation and Development (LaDOTD) SHL-vehicle permit LA-8T-14, for example, shows similar axles evenly distributed by a 4.6-ft spacing along the length of the SHL vehicle (see figure 23). In this case, all the axles can be treated as one group, and identifying the nucleus and average uniform σ_v (q_{ave}) on top of the SG layer can be initiated for this group. The entire SHL vehicle is, therefore, assumed to be the bearing capacity investigation zone (i.e., loaded area) applying q_{ave} .



© 2018 UNR.

Figure 23. Illustration. Example configuration (LA-8T-14) of an LaDOTD-permitted SHL vehicle (continuous axle configuration).

In the second category, an SHL vehicle consists of two or more dollies, the gaps between which are relatively large in comparison to the spacing between the axles within the dollies. As shown in figure 24, the SHL vehicle in the LA-12T-16 permit consists of 4 individual dollies where each dolly has 6 axles and 12 tires per axle, and the spacing between the dollies is nearly 38 ft. Each dolly should be considered one group, so there are a total of four groups in this case. The nucleus and q_{ave} on top of the SG layer for one axle group (i.e., one dolly) should be used for investigating the bearing capacity since the four axle groups are identical. In this case, the loaded area is constrained to the length and width of one dolly.



© 2018 UNR.

Figure 24. Illustration. Example configuration (LA-12T-16) of an LaDOTD-permitted SHL vehicle (fragmented axle configuration).

The third category covers general cases with any axle and tire configuration. Figure 25 shows a schematic of an SHL-vehicle configuration retrieved from a Nevada Department of Transportation (NDOT) permit. This permit encompasses cases with different axles (single, tandem, and tridem) with spacings. As such, there are many axle groups in this category, and each group can have an individual nucleus and q_{ave} on top of an SG layer. Therefore, each axle group is assumed to be a bearing capacity investigation zone. Detailed discussions regarding axle grouping and processes for nucleus identification are presented in Volume III: Appendix B.⁽³⁾

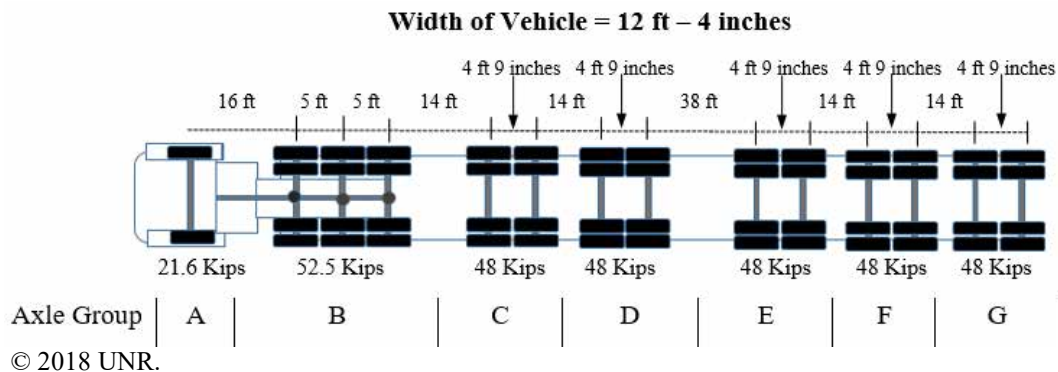


Figure 25. Illustration. Example configuration of an NDOT-permitted SHL vehicle.

Meyerhof's q_u equation requires the loaded area to be a fixed shape (e.g., circle or rectangle) with a uniform pressure distribution. As presented in figure 26, q_{ave} induced by a nucleus can be calculated by taking the integral of the σ_v distribution induced by the nucleus on top of the SG layer and then dividing it by the affected area ($A_{affected}$).

$$q_{ave} = \frac{\int \sigma_v \cdot dx \cdot dy}{A_{affected}}$$

Figure 26. Equation. Calculation of q_{ave} .

Where:

dx = differential of the variable x .

dy = differential of the variable y .

The conservative assumption that q_{ave} covers the entire rectangular area of the axle group generates the worst-case scenario regarding stress distribution. A smaller set of tires or axles may be assumed to be the bearing capacity investigation zone. Because it is impossible for one part of the SHL vehicle to develop a general bearing capacity failure mechanism while the rest of the vehicle does not, a failure area cannot be subdivided. An SHL vehicle moves as a unit, and load redistribution will take place when one part of the vehicle undergoes large deformations.

2.3. SHL-VEHICLE CASES

The SHL-vehicle cases presented in Volume III: Appendix B (namely case number (No.) 2, LA-8T-14) were selected to present the application of Meyerhof's q_u equation for the investigation of instantaneous shear failure under an SHL-vehicle movement.⁽³⁾ The SHL vehicle in case No. 2 had 28 line axles and 8 tires per axle; because the SHL vehicle consisted of uniformly spaced axles, it had only one axle group. This case was selected because it contained the maximum tire load and GVW among the 16 SHL-vehicle permits received from the LaDOTD truck permit office. The GVW was over 3.6 million lb with a tire load of 16,342 lb (see figure 27).

3D-Move Analysis was the software chosen to compute the stress distributions within the pavement structure.⁽²¹⁾ This software calculates pavement responses at selected depths within a pavement structure as a function of axle and load configurations, pavement structure, and material properties.

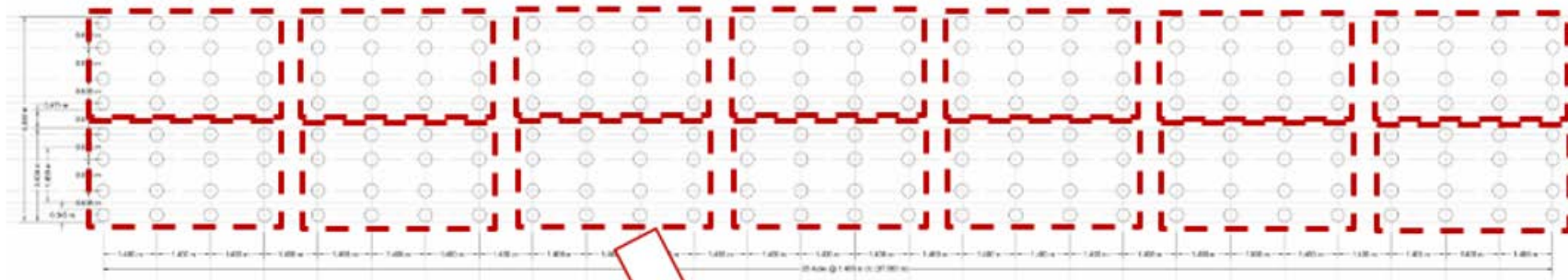
2.3.1. 3D-Move Analysis Inputs

The load input in 3D-Move Analysis includes six options, which cover most of the commonly used load configurations, to specify the stress distribution of tire-pavement contact.⁽²¹⁾ This software is capable of handling multiple load combinations with loaded areas of virtually any shape. In one of the input options, the user can manually upload a load-input file that allows for any loaded area with nonuniform, normal tire-pavement contact stress distribution and nonuniform interface shear stresses caused by braking and turning forces.⁽²¹⁻²³⁾ In the analysis results presented in section 2.3.2, a uniformly distributed circular load configuration was used with a uniform tire pressure of 120 psi.

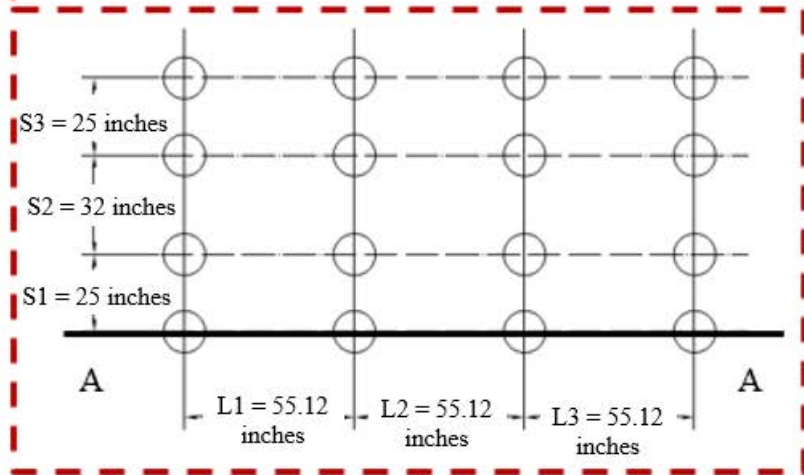
The pavement structure used for the ultimate failure analysis consisted of 9 inches of asphalt concrete (AC) on top of 10 inches of crushed aggregate base (CAB) and a semi-infinite SG layer. Figure 28 shows a three-dimensional (3D) schematic of the pavement structure. The viscoelastic properties of the AC layer were characterized using the dynamic modulus (E^*) laboratory data and asphalt-binder properties as a function of temperature and frequency. 3D-Move Analysis

generates E^* master curves at any reference temperature.⁽²¹⁾ The AC behavior was considered linear viscoelastic, while unbound materials (CAB and SG) were assumed to behave as linear elastic. Table 2 lists the material properties of each layer, and table 3 and table 4 show the selected viscoelastic properties of the AC material E^* and phase angle, respectively. E^* data are for a typical dense-graded hot-mix asphalt (HMA) with a performance grade (PG) 64-22 unmodified asphalt binder.¹

¹This is from an unpublished internal 2014 FHWA report, *Analysis Procedures for Evaluating Superheavy Load Movement on Flexible Pavements*.

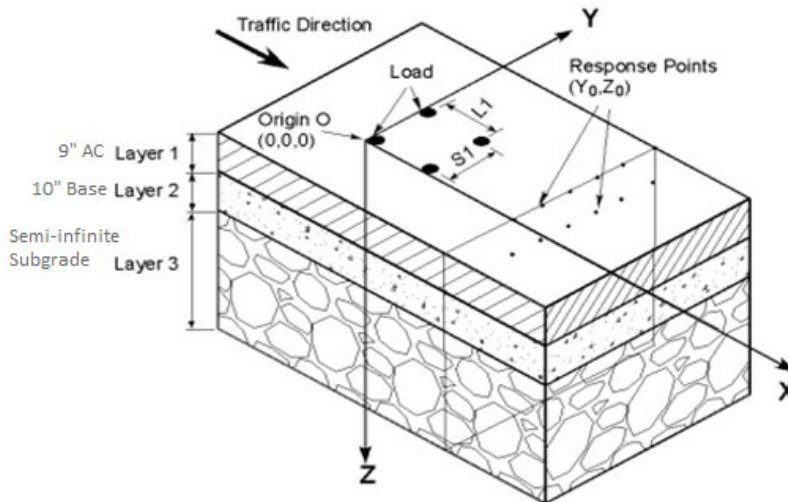


8 Tires x 28 Axles
 Tire Load = 16,342 lb
 GVW = 3,660,552 lb



© 2018 UNR.
 L1, L2, and L3 = distance between axles.
 S1, S2, and S3 = distance between tires.

Figure 27. Illustration. SHL-vehicle axle configuration (case No. 2: LA-8T-14) and nucleus of SHL configuration.



© 2018 UNR.
L1= distance between axes.
S1 = distance between tires.

Figure 28. Illustration. 3D schematic of the pavement structure in 3D-Move Analysis.⁽²¹⁾

Table 2. Material properties of each layer.

Layer No.	Layer Type	Material	Thickness (Inches)	Unit Weight (pci)	Poisson's Ratio	Resilient Modulus (psi)
1	AC	Linear viscoelastic	9	0.08	0.40	*
2	CAB	Linear elastic	10	0.06	0.40	30,000
3	SG	Linear elastic	240	0.06	0.45	5,000

*The resilient modulus for layer 1 is variable and depends on frequency.

Table 3. E^* values for a typical dense-graded HMA with PG64-22.

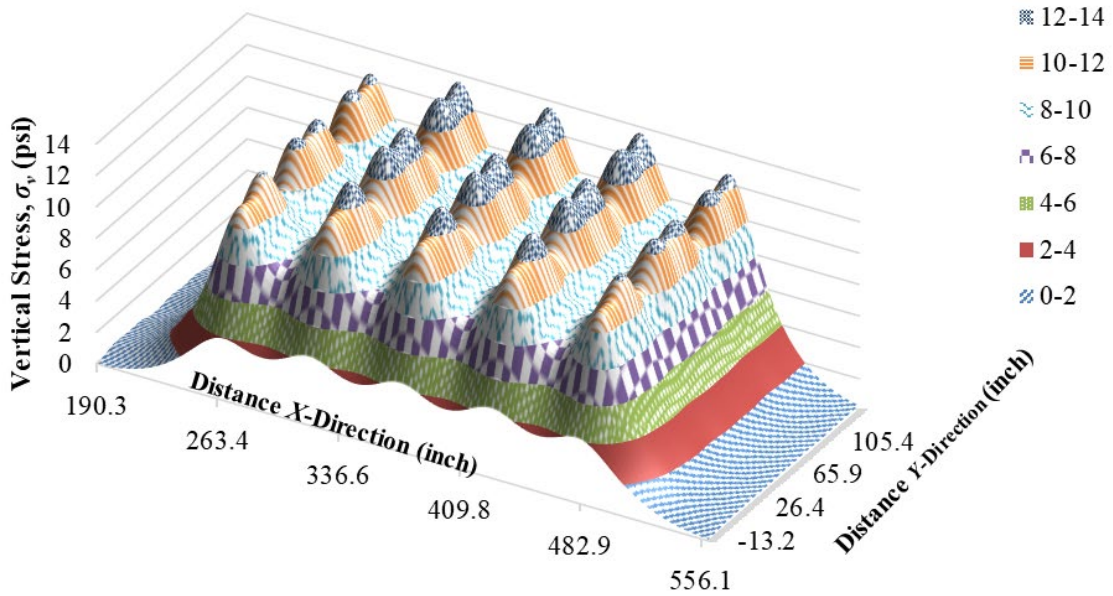
Temperature (°F)	E^* at 0.1 Hz (psi)	E^* at 0.5 Hz (psi)	E^* at 1 Hz (psi)	E^* at 5 Hz (psi)	E^* at 10 Hz (psi)	E^* at 25 Hz (psi)
40	693,889	1,012,294	1,163,463	1,530,813	1,690,524	1,898,005
70	141,296	262,736	334,941	554,052	670,382	842,418
100	21,439	45,076	61,705	123,984	164,420	233,925
130	4,025	7,934	10,801	22,592	31,147	47,465

Table 4. Phase angle values for a typical dense-grade HMA with PG64-22.

Temperature (°F)	Phase Angle at 0.1 Hz (Degrees)	Phase Angle at 0.5 Hz (Degrees)	Phase Angle at 1 Hz (Degrees)	Phase Angle at 5 Hz (Degrees)	Phase Angle at 10 Hz (Degrees)	Phase Angle at 25 Hz (Degrees)
40	22.1	19.0	17.3	15.5	15.9	18.1
70	31.2	29.8	30.1	27.8	27.4	26.3
100	28.5	29.9	31.3	35.0	35.5	36.8
130	23.2	26.8	27.0	33.9	34.1	40.1

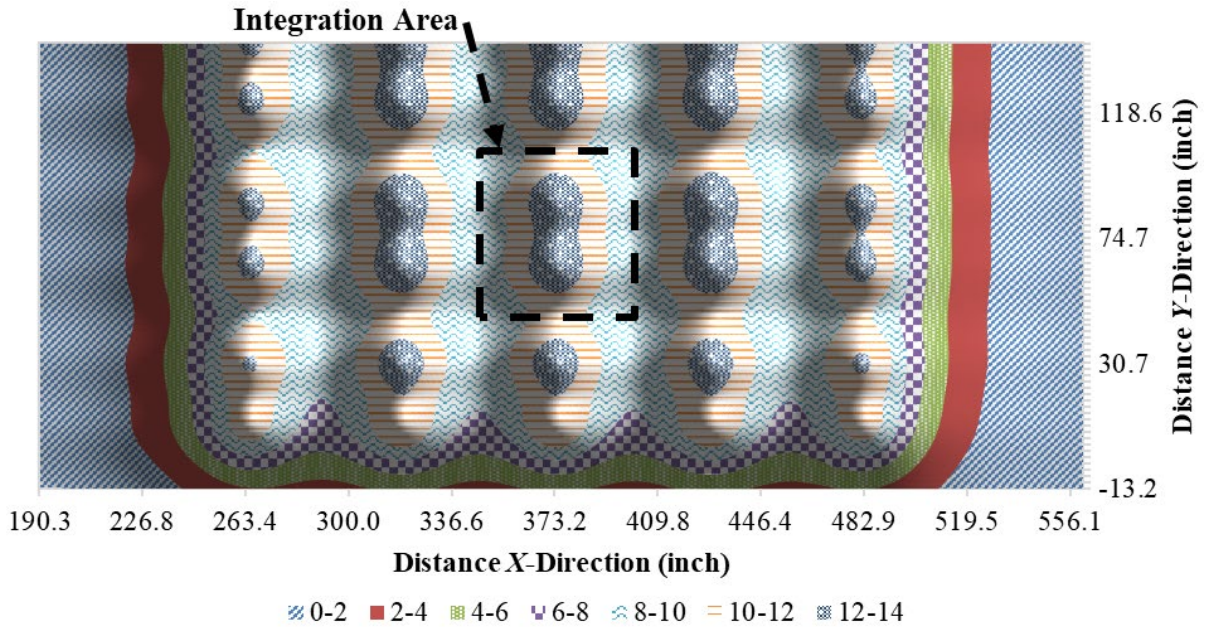
2.3.2. Determination of q_{ave}

Figure 29 presents the computed σ_v distribution on top of the SG layer. In case No. 2, q_{ave} equaled 10.5 psi, which was calculated by dividing the volume by the area of the integration area (see figure 30 and figure 31).



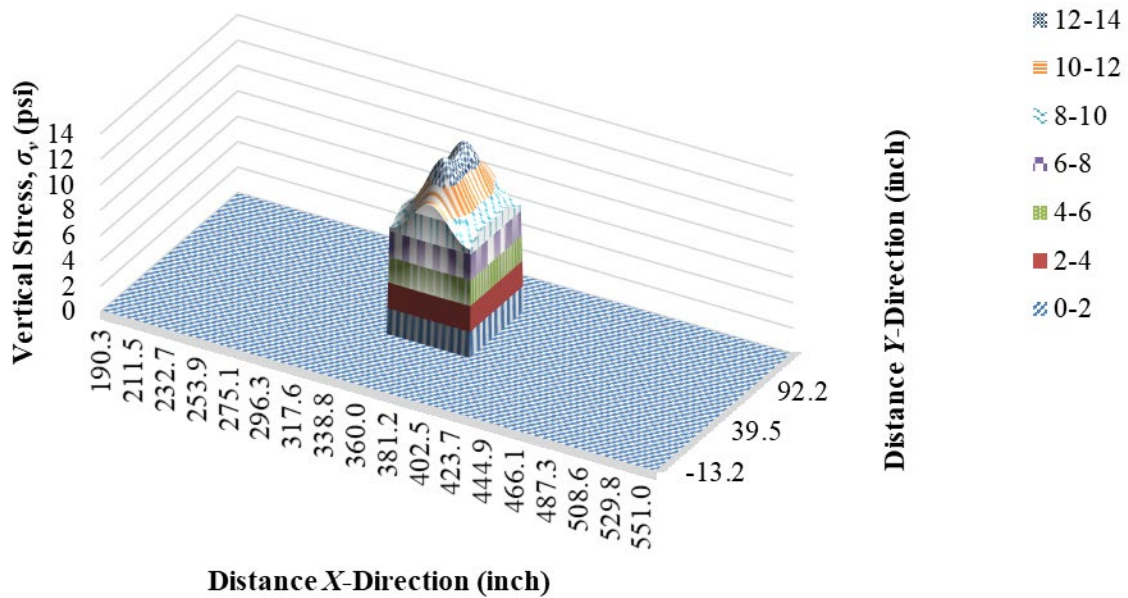
© 2018 UNR.

Figure 29. Chart. 3D view of σ_v distribution on top of the SG with five axles with six tires each (SHL case No. 2: LA-8T-14, 100°F).



© 2018 UNR.

Figure 30. Chart. Top view of σ_v distribution on top of the SG with five axles with six tires each (SHL case No. 2: LA-8T-14, 100 °F).



© 2018 UNR.

Figure 31. Chart. 3D view of σ_v distribution at middle dual tires on top of the SG (SHL case No. 2: LA-8T-14, 100 °F).

2.3.3. Bearing Capacity Failure Analysis

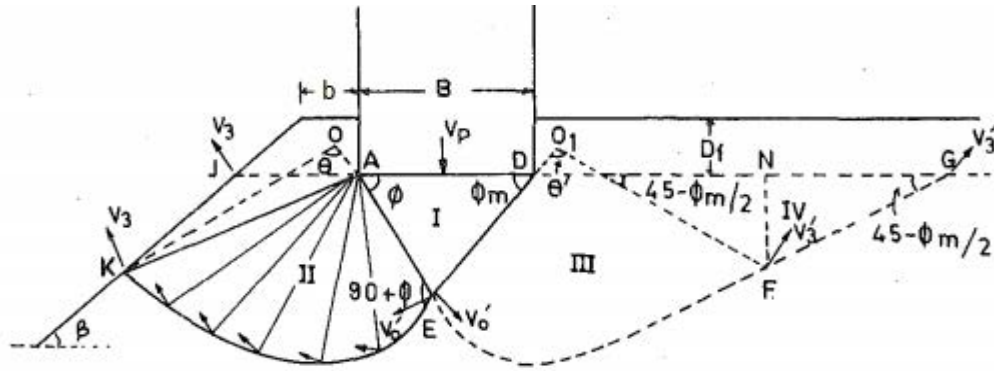
For this analysis, the shear strength parameters of the SG soil (ϕ and c) were estimated for a soil with a resilient modulus of 5,000 psi using the following suggested values from other literature: $c = 1.5$ psi and $\phi = 26$ degrees.^(24,25)

Meyerhof's q_u equation was used to estimate the bearing capacity of the SG soil. In case No. 2, the investigation zone for bearing capacity was the entire SHL vehicle because it had only one axle group. q_u was calculated as 54.2 psi (see figure 2). The factor of safety (FOS) against the bearing capacity failure was then calculated as the ratio of q_u to q_{ave} . Knowing that q_{ave} is 10.5 psi, FOS against bearing capacity was calculated as 5.1.

2.4. BEARING CAPACITY ASSOCIATED WITH SLOPING SHOULDER

Volume VII: Appendix F elaborates on the limit state analysis used to investigate the stability of a sloped pavement shoulder.⁽⁶⁾ The failure mode in which the pavement layers, along with the surface loading from the SHL vehicle, undergo failure as a single unit may be important. This condition is analogous to the slope stability investigation of shallow strip foundations placed on top of the flat surface of a side sloping ground. Meyerhof combined the bearing capacity theory with the theory of slope stability to account for foundations on slopes. However, his solution was purely for cohesive or purely granular soils.^(26,27) Saran et al. provided a solution to determine the ultimate bearing capacity of a shallow strip foundation on a slope using the limit equilibrium and limit analysis considering a one-sided failure mechanism, as shown in figure 32.⁽²⁷⁾ Saran et al. indicated the failure mechanism in the foundation soil on a slope is affected by soil type.

According to this theory, the ultimate bearing capacity for a shallow strip foundation is given by the equation shown in figure 33.



© 1989 with permission from the American Society of Civil Engineers.

B = width (or diameter) of the foundation.

b = distance from the edge of the slope.

D_f = depth of the foundation measured from the ground surface.

V_0' = velocity of soil in the transition zone at point E on the side without slope.

V_3 = velocity of soil at the end of transition zone.

V_3' = velocity of soil at the end of log spiral on the side without slope.

V_p = velocity of foundation.

β = inclination of the slope.

θ = logarithmic spiral angle.

ϕ = angle of internal friction.

ϕ_m = mobilized angle of internal friction.

Figure 32. Chart. Bearing capacity failure under a rough rigid foundation on a slope.⁽²⁷⁾

$$q_u = (c)(Nc) + (\bar{q})(Nq) + \left(\frac{1}{2}\gamma\right)(B)(N\gamma)$$

Figure 33. Equation. Calculation of ultimate bearing capacity for a shallow strip foundation.

The values of Nc , Nq , and $N\gamma$ need to be modified to consider the presence of the slope. These factors are given in table 5 through table 7 as a function of the inclination of the slope (β), distance from the edge of the slope (b), D_f , ϕ , and B , all as shown in figure 32. In this study, Saran et al.'s approach was adopted to investigate the bearing capacity failure under an SHL-vehicle movement on a flexible pavement with a sloped shoulder.⁽²⁷⁻³¹⁾

Table 5. N_c associated with a sloped shoulder.

β (Degrees)	D/B	b/B	$\phi =$ 40 Degrees	$\phi =$ 35 Degrees	$\phi =$ 30 Degrees	$\phi =$ 25 Degrees	$\phi =$ 20 Degrees	$\phi =$ 15 Degrees	$\phi =$ 10 Degrees
50	0	0	21.68	16.52	12.60	10.00	8.6	7.10	5.50
40	0	0	31.80	22.44	16.64	12.80	10.04	8.00	6.25
30	0	0	44.80	28.72	22.00	16.20	12.2	8.60	6.70
20	0	0	63.20	41.20	28.32	20.60	15	11.30	8.76
≤ 10	0	0	88.96	55.36	36.50	24.72	17.36	12.61	9.44
50	0	1	38.80	30.40	24.20	19.70	16.42	—	—
40	0	1	48.00	35.40	27.42	21.52	17.28	—	—
30	0	1	59.64	41.07	30.92	23.60	17.36	—	—
20	0	1	75.12	50.00	35.16	27.72	17.36	—	—
≤ 10	0	1	95.20	57.25	36.69	24.72	17.36	—	—
50	1	0	35.97	28.11	22.38	18.38	15.66	10.00	—
40	1	0	51.16	37.95	29.42	22.75	17.32	12.16	—
30	1	0	70.59	50.37	36.20	24.72	17.36	12.16	—
20	1	0	93.79	57.20	36.20	24.72	17.36	12.16	—
≤ 10	1	0	95.20	57.20	36.20	24.72	17.36	12.16	—
50	1	1	53.65	42.47	35.00	24.72	—	—	—
40	1	1	67.98	51.61	36.69	24.72	—	—	—
30	1	1	85.30	57.25	36.69	24.72	—	—	—
≤ 20	1	1	95.20	57.25	36.69	24.72	—	—	—

—No data.

Table 6. Nq associated with a sloped shoulder.

β (Degrees)	D/B	b/B	$\phi =$ 40 Degrees	$\phi =$ 35 Degrees	$\phi =$ 30 Degrees	$\phi =$ 25 Degrees	$\phi =$ 20 Degrees	$\phi =$ 15 Degrees	$\phi =$ 10 Degrees
30	1	0	12.13	16.42	8.98	7.04	5.00	3.60	—
20	1	0	12.67	19.48	16.80	12.70	7.40	4.40	—
≤ 10	1	0	81.30	41.4	22.50	12.70	7.40	4.40	—
30	1	1	28.31	24.14	22.50	—	—	—	—
20	1	1	42.25	41.40	22.50	—	—	—	—
≤ 10	1	1	81.30	41.40	22.50	—	—	—	—

—No data.

Table 7. Ny associated with a sloped shoulder.

β (Degrees)	D/B	b/B	$\phi =$ 40 Degrees	$\phi =$ 35 Degrees	$\phi =$ 30 Degrees	$\phi =$ 25 Degrees	$\phi =$ 20 Degrees	$\phi =$ 15 Degrees	$\phi =$ 10 Degrees
30	0	0	25.37	12.41	6.14	3.20	1.26	0.70	0.10
20	0	0	53.48	24.54	11.62	5.61	4.27	1.79	0.45
10	0	0	101.74	43.35	19.65	9.19	4.35	1.96	0.77
0	0	0	165.39	66.59	28.98	13.12	6.05	2.74	1.14
30	0	1	60.06	34.03	18.95	10.33	5.45	0	—
20	0	1	85.98	42.29	21.93	11.42	5.89	1.35	—
10	0	1	125.32	55.15	25.86	12.26	6.05	2.74	—
0	0	1	165.39	66.59	28.89	13.12	6.05	2.74	—
30	1	0	91.87	49.43	26.39	—	—	—	—
25	1	0	115.65	59.12	28.80	—	—	—	—
20	1	0	143.77	66.00	28.89	—	—	—	—
≤ 15	1	0	165.39	66.59	28.89	—	—	—	—
30	1	1	131.34	64.37	28.89	—	—	—	—
25	1	1	151.37	66.59	28.89	—	—	—	—
≤ 20	1	1	166.39	66.59	28.89	—	—	—	—

—No data.

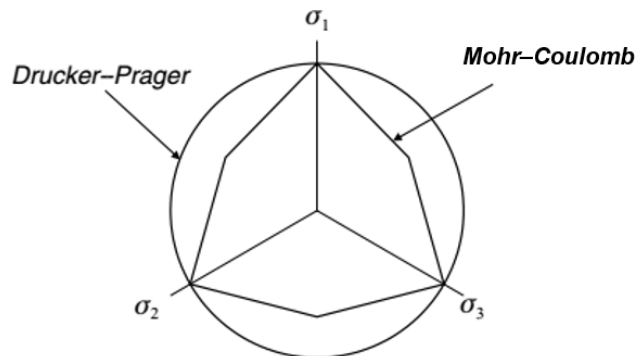
CHAPTER 3. SERVICE LIMIT ANALYSES

This chapter presents the service limit analyses conducted for a flexible pavement under an SHL-vehicle movement. These analyses include a localized shear failure analysis and deflection-based analysis. The comparison of a load-induced stress level on top of an SG layer to the corresponding strength criterion for that layer is carried out to investigate the localized shear failure (local instability). Mitigation strategies might be required if this analysis indicates a possibility for failure. If a low possibility is determined, a subsequent evaluation of the surface displacement (deflection) is performed. This evaluation, which is referred to as a deflection-based service limit analysis, is conducted since excessive load-induced surface deflection can result in early deterioration of the pavement structure.

3.1. LOCALIZED SHEAR FAILURE ANALYSIS UNDER SHL-VEHICLE MOVEMENTS

As presented in figure 1, ultimate failure analyses, which are elaborated on in chapter 2, are essential first steps for evaluating the risk of shear failure in the SG layer of a pavement structure subjected to an SHL-vehicle movement. Once these analyses confirm the structure has an adequate bearing capacity, the likelihood for the onset of yielding in the SG layer due to localized shear failure is examined. The focus of the localized shear failure analysis is placed on the substantial load-induced state of stresses developed in the pavement structure that might reach a state close to failure. In this study, the localized shear failure analysis focused on the SG layer, which typically represents the most vulnerable pavement layer, as it has the lowest strength.

Numerous failure criteria, such as Mohr–Coulomb, Drucker–Prager, Lade–Duncan, and Matsuoka–Nakai, have been proposed for evaluating the yielding (i.e., failure) of soil materials.⁽³²⁾ The Drucker–Prager yield criterion (figure 34), which involves ϕ and c of the soil material, is a well-accepted criterion in soil plasticity. The Drucker–Prager yield criterion presented in figure 34 includes the Mohr–Coulomb yield criterion for 3D stress states. The equation in figure 35 represents the Drucker–Prager yield criterion.



© 2018 UNR.

σ_1 , σ_2 , and σ_3 = major, intermediate, and minor principal stresses, respectively.

Figure 34. Illustration. Drucker–Prager and Mohr–Coulomb yield surfaces.

$$q - \zeta p - \kappa = 0$$

Figure 35. Equation. Drucker–Prager yield criterion.

Where:

q = deviator stress in Drucker–Prager yield criterion.

ζ = Drucker–Prager material constant associated with ϕ .

p = mean normal stress in Drucker–Prager yield criterion.

κ = Drucker–Prager material constant associated with ϕ and c .

ζ and κ are expressed in terms of ϕ and c , as shown in figure 36 and figure 37. In addition, q and p can be written as a function of the second invariant of the deviator stress tensor (\bar{I}_{2D}) and first invariant of the stress tensor (I_1), as shown in figure 38 and figure 39, respectively.

$$\zeta = \frac{6\sin\phi}{3 - \sin\phi}$$

Figure 36. Equation. Calculation of ζ .

$$\kappa = \frac{6c \cos\phi}{3 - \sin\phi}$$

Figure 37. Equation. Calculation of κ .

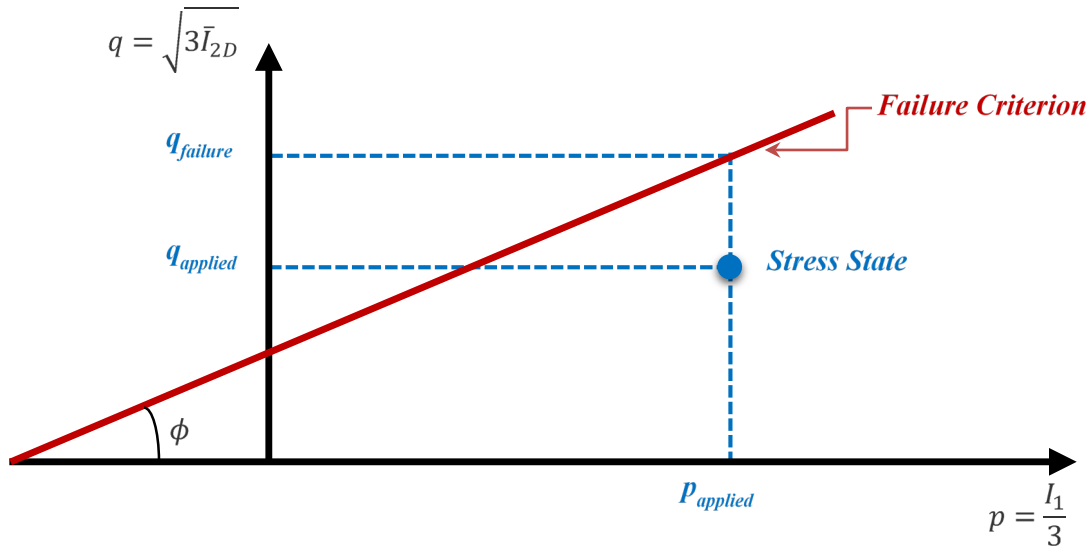
$$q = \sqrt{3\bar{I}_{2D}}$$

Figure 38. Equation. Calculation of q .

$$p = \frac{I_1}{3}$$

Figure 39. Equation. Calculation of p .

The Drucker–Prager yield criterion is a straight line on the q versus p (i.e., $q-p$) plot. Figure 40 demonstrates the Drucker–Prager failure envelope in the $q-p$ plot. As presented in this figure, at a certain induced mean normal stress ($p_{applied}$), FOS is defined as the ratio of the Drucker–Prager deviator stress at failure ($q_{failure}$) and induced deviator stress ($q_{applied}$) (see figure 41). FOS is an indication of how far the stress state is from the failure envelope and can be rewritten as a function of ζ and κ , as presented in figure 42.



© 2018 UNR.

Figure 40. Chart. Representation of the Drucker–Prager yield criterion in the q – p plot.

$$FOS = \frac{q_{failure}}{q_{applied}}$$

Figure 41. Equation. Calculation of FOS using the Drucker–Prager yield criterion.

$$FOS = \frac{\xi p_{applied} + \kappa}{q_{applied}}$$

Figure 42. Equation. Calculation of FOS as a function of ξ and κ .

For the conventional triaxial test, q and p are measured directly. $p_{applied}$ and $q_{applied}$ of an SHL vehicle can be determined by transforming the computed stress tensor (σ_{ij}) to the equivalent triaxial testing condition using figure 38 and figure 39. Subsequently, FOS against localized shear failure for a pavement structure subjected to an SHL-vehicle movement is determined. The following steps outline the proposed approach:

1. The identified nucleus of the SHL-vehicle and the representative moduli for the pavement layers are used to calculate σ_{ij} at the critical locations on top of the SG where a higher possibility for localized shear failure exists. The selection of critical locations is then provided. For cases where SHL vehicles comprise two or more axle groups, the critical axle group is selected for the analysis. The critical axle group includes the nucleus that induces the highest σ_v on top of the SG layer. The procedures to determine the nucleus of an SHL vehicle with different axle and tire configurations as well as representative moduli for the pavement layers are elaborated in Volume III: Appendix B and Volume IV: Appendix C, respectively.^(3,4)
2. The calculated load-induced σ_{ij} at the critical locations on top of the SG is transformed into equivalent stresses in laboratory triaxial testing conditions by using stress invariants in a way that is similar to previous studies.^(23,33) The octahedral normal stress (σ_{oct}) and

shear stress (τ_{oct}), which are invariants, are used to calculate the load-induced $p_{applied}$ and $q_{applied}$, respectively, using the equations in figure 43 through figure 46. In these equations, σ_1 , σ_2 , and σ_3 are the major, intermediate, and minor principal stresses induced by the SHL-vehicle movement, respectively.

3. Knowing ϕ and c of the SG layer, as well as the computed $p_{applied}$ and $q_{applied}$ under the SHL-vehicle movement, FOS against localized shear failure is calculated using figure 42. FOS less than 1 indicates failure at the location of consideration.

$$\sigma_{oct} = \frac{1}{3}(\sigma_1 + \sigma_2 + \sigma_3)$$

Figure 43. Equation. Calculation of σ_{oct} using principal stresses.

$$|\tau_{oct}| = \frac{1}{3}\sqrt{(\sigma_1 - \sigma_2)^2 + (\sigma_2 - \sigma_3)^2 + (\sigma_3 - \sigma_1)^2}$$

Figure 44. Equation. Calculation of τ_{oct} using principal stresses.

$$p_{applied} = \sigma_{oct}$$

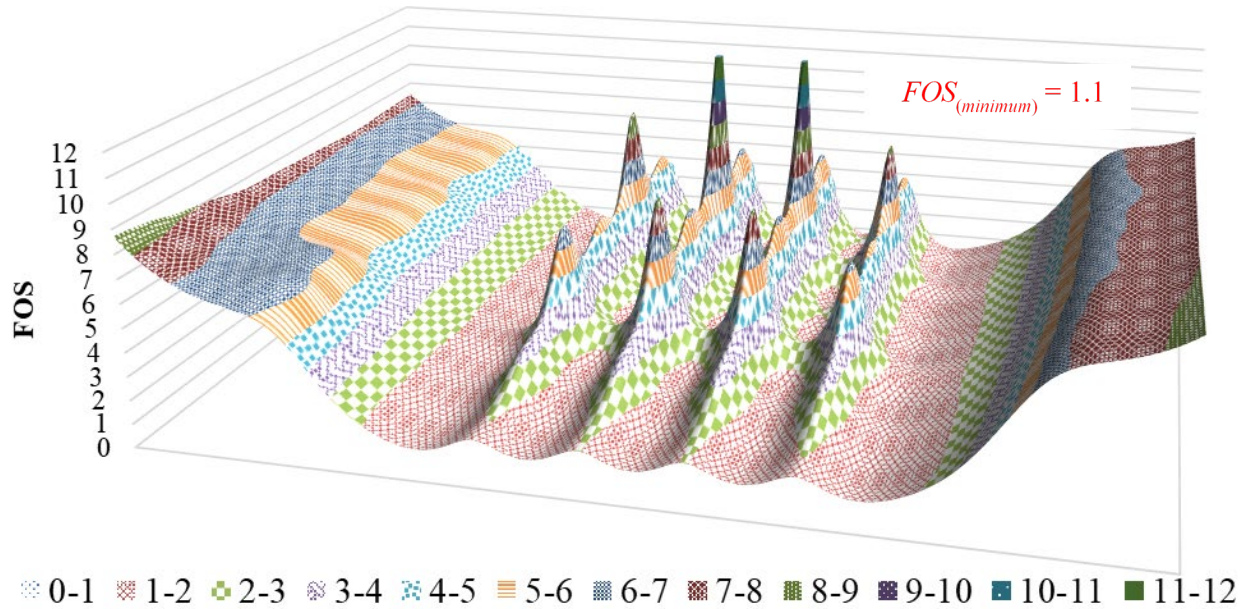
Figure 45. Equation. Calculation of $p_{applied}$ using σ_{oct} .

$$q_{applied} = \frac{3}{\sqrt{2}}|\tau_{oct}|$$

Figure 46. Equation. Calculation of $q_{applied}$ using τ_{oct} .

In a triaxial test, decreasing the confining stress (σ_c) and/or increasing the deviator stress (σ_d) represents the state of the stresses closer to the failure state. For a moving surface load, the stress tensor varies within the SG layer. Therefore, the highest possibility for a localized shear failure (corresponding to the lowest FOS) is at locations where the lowest triaxial equivalent σ_c and highest σ_d are calculated. For an SHL-vehicle movement, one critical location can be the middle of the nucleus where σ_v reaches a maximum value. As the edge of the nucleus experiences the lowest σ_c , making it prone to shear failure, this can be considered another critical location as well.

Figure 47 shows the 3D surface plot for FOS determined at the SG layer of the pavement structure in SHL case No. 2. The SHL-vehicle axle and tire configurations, pavement structure, and material properties for SHL case No. 2 are presented in section 2.3 of this report. Figure 47 implies that a minimum FOS (i.e., the highest possibility for a localized shear failure) is at the edge of the SHL vehicle's nucleus. 3D-Move ENHANCED, which is incorporated into the Superheavy Load Pavement Analysis PACKage (SuperPACK), is capable of providing a 3D surface plot at any depth of interest.^(9,34) Therefore, the critical location at the top of the SG and subsequent minimum FOS can be readily identified by SuperPACK.⁽⁹⁾



© 2018 UNR.

$FOS_{(minimum)}$ = minimum FOS .

Figure 47. Chart. FOS for the SHL-vehicle nucleus.

3.2. DEFLECTION-BASED SERVICE LIMIT ANALYSIS UNDER SHL-VEHICLE MOVEMENTS

The failure analyses investigate the likelihood of shear failure in the SG layer of a pavement structure in both global and localized manners. The results of these analyses can reveal whether or not the pavement structure is capable of withstanding the loading of an SHL-vehicle movement without experiencing shear failure.

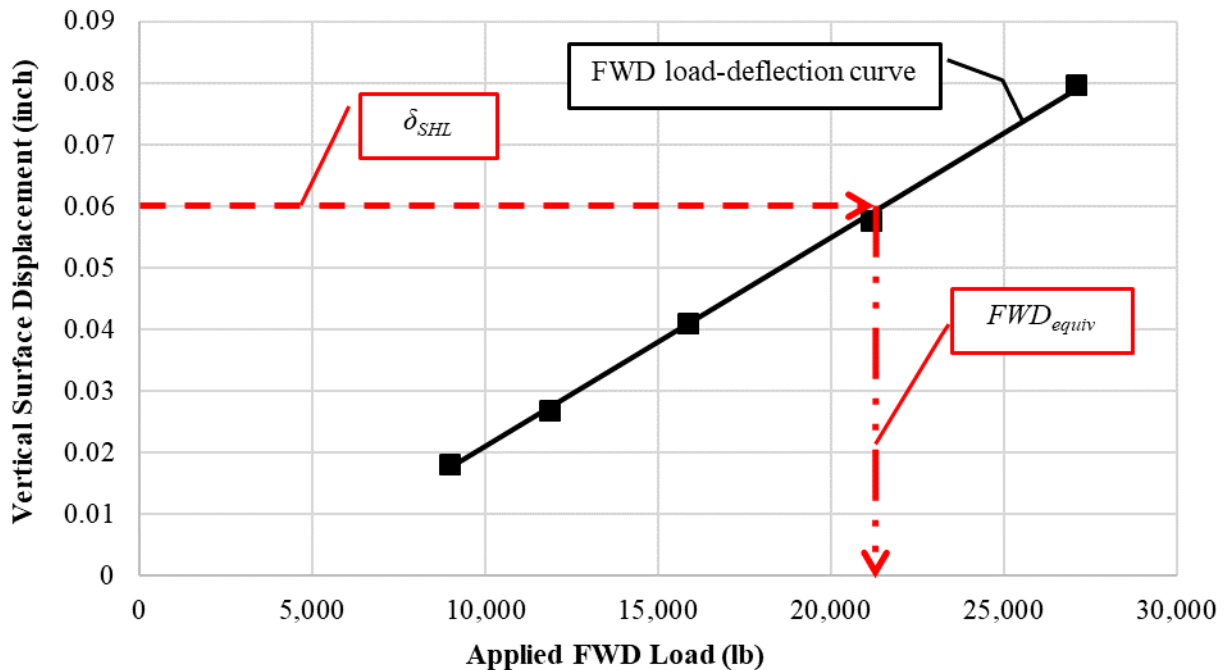
Pavement structures might encounter excessive surface deflections, which can lead to the development of premature surface distresses and rapid deterioration under SHL-vehicle movements. To prevent excessive surface deflections from occurring, SHL vehicle-induced surface deflections (δ_{SHL}) should be determined and limited to a certain allowable deflection. In the proposed deflection-based service limit analysis, an equivalent falling weight deflectometer (FWD)-load level (FWD_{equiv}), which generates a center deflection at the center of the FWD plate (D_0) equal to δ_{SHL} , is determined. In other words, the equivalency is established between the SHL-vehicle load and the FWD load level (i.e., FWD_{equiv}) based on the same induced surface deflection. Subsequently, FWD_{equiv} is compared to an allowable FWD load level (FWD_{allow}). FWD_{equiv} higher than FWD_{allow} indicates a need for mitigation strategies.

The remainder of this chapter details the steps associated with the deflection-based service limit analysis. FWD data at multiple load levels (e.g., 9,000; 12,000; 16,000; 21,000; and 27,000 lb) are necessary inputs for this analysis.

3.2.1. Determination of FWD_{equiv}

The following list describes the major steps developed as part of this study to determine FWD_{equiv} under an SHL-vehicle movement:

1. The identified critical nucleus of an SHL vehicle and representative moduli of the pavement layers are used to calculate δ_{SHL} . The procedures to determine the critical nucleus of an SHL-vehicle movement and representative moduli of the pavement layers are elaborated in Volume III: Appendix B and Volume IV: Appendix C, respectively.^(3,4)
2. The FWD load–deflection curve is developed using D_0 measurements at multiple FWD load levels (see figure 48). However, the temperature of the AC layer at the time of the SHL-vehicle movement may be different from the temperature when the FWD testing was conducted. Therefore, the measured D_0 needs to be adjusted to the analysis temperature (i.e., the AC layer temperature at the time of the SHL-vehicle movement). To accomplish this, the AC layer stiffness at the analysis temperature is determined using the field damaged E^* master curve and FWD loading frequency. Details to establish the field damaged E^* master curve of the existing AC layer are presented in Volume IV: Appendix C.⁽⁴⁾ Accordingly, surface deflections at different FWD load levels are calculated using the determined AC layer stiffness (i.e., temperature-adjusted stiffness) along with the backcalculated resilient moduli of the unbound layers at the corresponding FWD load level using the static loading condition in 3D-Move ENHANCED.⁽³⁴⁾
3. Using the calculated δ_{SHL} and developed FWD load–deflection curve from step 2, FWD_{equiv} to the SHL-vehicle load is identified, as illustrated in figure 48.



© 2018 UNR.

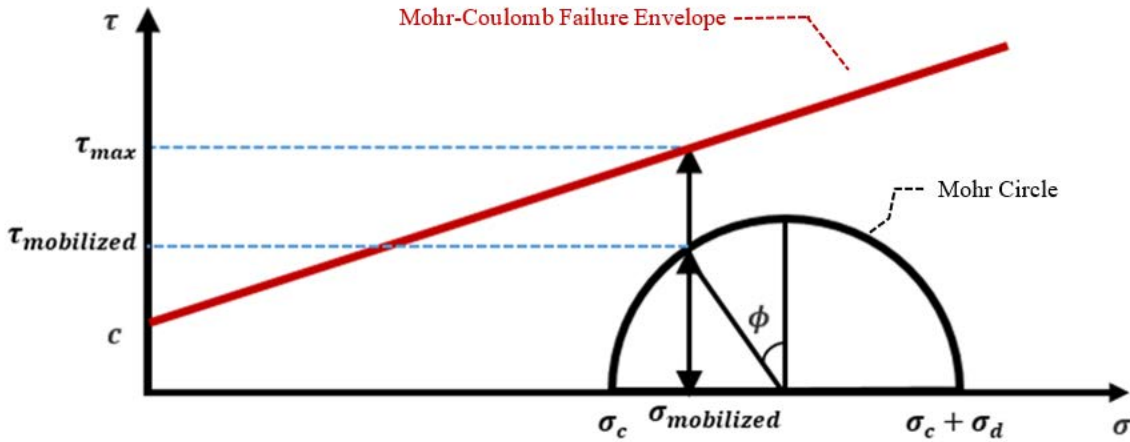
Figure 48. Chart. FWD load–deflection curve.

3.2.2. Determination of FWD_{allow}

Previous studies reported that permanent deformation in unbound materials (e.g., CAB and SG) could be reasonably assessed by means of the shear stress ratio (SSR) concept.^(35–38) In other words, a limited SSR value can be used as a control for the permanent deformation in the unbound materials. As illustrated in figure 49 and figure 50, SSR is defined as the ratio between applied (mobilized) shear stress ($\tau_{mobilized}$) and maximum shear strength (τ_{max}) of the unbound material. Using the Mohr–Coulomb yield criteria, $\tau_{mobilized}$ and τ_{max} can be written as a function of ϕ and c , as shown in figure 51 and figure 52, respectively.

$$SSR = \frac{\tau_{mobilized}}{\tau_{max}}$$

Figure 49. Equation. Calculation of SSR.



© 2018 UNR.

Figure 50. Chart. Representation of τ_{max} and $\tau_{mobilized}$.

$$\tau_{mobilized} = \frac{\sigma_d \cos(\phi)}{2}$$

Figure 51. Equation. Calculation of $\tau_{mobilized}$.

$$\tau_{max} = \left(\frac{2\sigma_c + \sigma_d}{2} - \frac{\sigma_d \sin(\phi)}{2} \right) \tan(\phi) + c$$

Figure 52. Equation. Calculation of τ_{max} .

In this study, the concept of SSR was employed to determine FWD_{allow} . When unbound materials experience SSR values higher than 0.7, high permanent strain accumulates in the materials, resulting in permanent deformation.^(35–38) The FWD load level that induces an SSR value equal to 0.7 at the top of the SG layer is identified as FWD_{allow} . The following summarizes the steps to determine FWD_{allow} :

1. Calculate σ_{ij} under each FWD load level (e.g., from 9,000 to 27,000 lb in increments of 3,000 lb) using 3D-Move ENHANCED.⁽³⁴⁾ This step uses the AC layer stiffness at the analysis temperature predetermined using the field damaged E^* master curve along with

the backcalculated resilient moduli of the unbound layers at each respective FWD load level. The point of interest is located below the center of the FWD loading plate and on top of the SG layer.

2. Calculate the load-induced σ_{oct} and τ_{oct} for each FWD load level using figure 43 and figure 44, respectively, and the calculated load-induced σ_{ij} values from step 1.
3. Calculate the equivalent laboratory triaxial σ_d and σ_c for each FWD load level using figure 53 and figure 54, respectively.

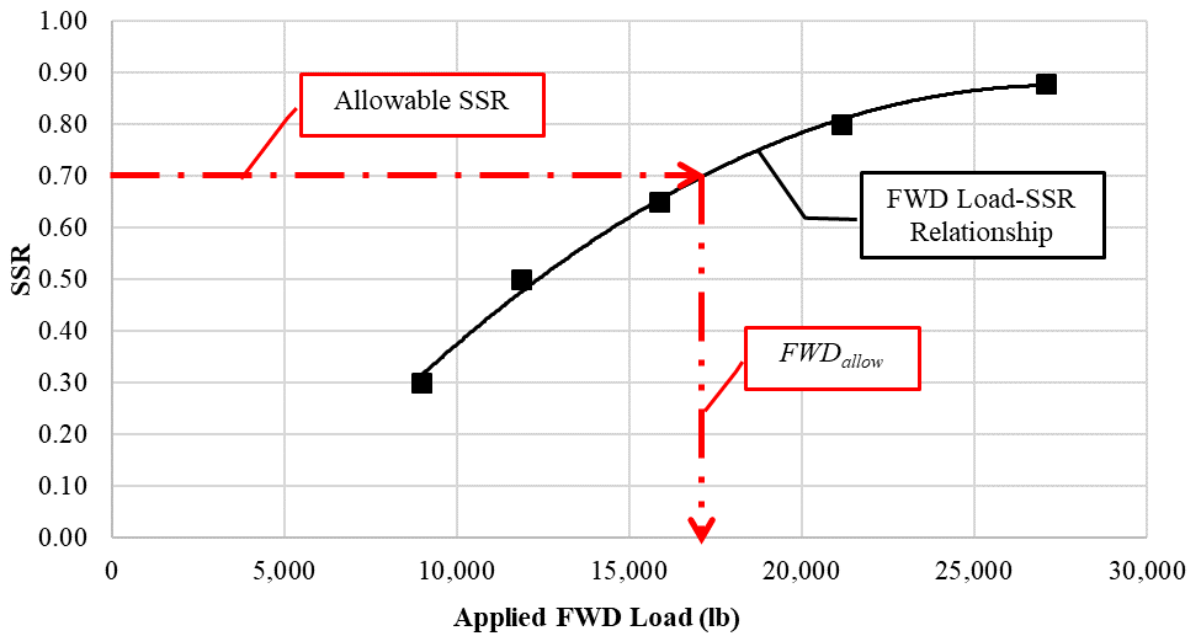
$$\sigma_d = \frac{3}{\sqrt{2}} |\tau_{oct}|$$

Figure 53. Equation. Calculation of equivalent σ_d .

$$\sigma_c = \sigma_{oct} - \frac{\sigma_d}{3}$$

Figure 54. Equation. Calculation of equivalent σ_c .

4. Calculate $\tau_{mobilized}$ and τ_{max} at each FWD load level under consideration using figure 51 and figure 52, respectively, along with σ_d and σ_c from step 2. Calculate the SSR values at each FWD load level using figure 49.
5. Establish the FWD load–SSR curve by plotting the SSR values versus their respective FWD load levels. Identify FWD_{allow} that corresponds to an SSR value of 0.7, as illustrated in figure 55.



© 2018 UNR.

Figure 55. Chart. FWD load–SSR curve.

CHAPTER 4. SUMMARY

SHL vehicles are much larger in size and weight than standard vehicles and often require specialized trailers and hauling units. SHL-vehicle movements may sometimes approach loads of a few million pounds. Such nonstandard heavy loading can render a critical condition (i.e., distress mode) of instantaneous ultimate shear failure, localized shear failure, or excessive surface deflections in a pavement surface.

To examine the risk of instantaneous shear failure, Meyerhof's q_u equation was adopted. The ultimate failure analysis that focuses on the SG layer compares the distributed σ_v on top of the SG layer induced by an SHL-vehicle movement to the bearing capacity of the SG layer itself. When there is a sloping pavement shoulder, a modified bearing capacity approach is applied. Once the bearing capacity investigation confirms a pavement structure can adequately withstand general shear failure, the likelihood for onset of yielding in the SG layer due to localized shear failure is examined. In the localized shear failure investigation, the focus is on the substantially higher SHL load-induced state of stresses developed on top of the SG approaching the SG failure state. The Drucker–Prager yield criterion is used to evaluate the risk of localized shear failure by examining the stress level on top of SG using a q – p plot.

Though the shear failure analyses may reveal that a pavement structure is capable of sustaining an SHL-vehicle movement without experiencing any instantaneous shear failure, excessive surface deflections might be encountered under an SHL vehicle. Surface deflections can eventually lead to the development of premature surface distresses and rapid deterioration of the pavement. Accordingly, δ_{SHL} is limited to an allowable surface deflection using a deflection-based service limit analysis. FWD_{equiv} that generates D_0 equal to δ_{SHL} is determined. Subsequently, FWD_{equiv} is compared with FWD_{allow} . FWD_{equiv} higher than FWD_{allow} indicates that the SHL vehicle-induced surface deflections are in excess of the allowable surface deflections. Mitigation strategies may then be needed to reduce FWD_{equiv} and/or increase FWD_{allow} .

REFERENCES

1. Hajj, E.Y., Siddharthan, R.V., Nabizadeh, H., Elfass, S., Nimeri, M., Kazemi, S.F., Batioja-Alvarez, D.D., and Piratheepan, M. (2018). *Analysis Procedures for Evaluating Superheavy Load Movement on Flexible Pavements, Volume I: Final Report*, Report No. FHWA-HRT-18-049, Federal Highway Administration, Washington, DC.
2. Nimeri, M., Nabizadeh, H., Hajj, E.Y., Siddharthan, R.V., Elfass, S., and Piratheepan, M. (2018). *Analysis Procedures for Evaluating Superheavy Load Movement on Flexible Pavements, Volume II: Appendix A, Experimental Program*, Report No. FHWA-HRT-18-050, Federal Highway Administration, Washington, DC.
3. Nimeri, M., Nabizadeh, H., Hajj, E.Y., Siddharthan, R.V., and Elfass, S. (2018). *Analysis Procedures for Evaluating Superheavy Load Movement on Flexible Pavements, Volume III: Appendix B, Superheavy Load Configurations and Nucleus of Analysis Vehicle*, Report No. FHWA-HRT-18-051, Federal Highway Administration, Washington, DC.
4. Nabizadeh, H., Hajj, E.Y., Siddharthan, R.V., and Elfass, S. (2018). *Analysis Procedures for Evaluating Superheavy Load Movement on Flexible Pavements, Volume IV: Appendix C, Material Characterization for Superheavy Load Movement Analysis*, Report No. FHWA-HRT-18-052, Federal Highway Administration, Washington, DC.
5. Nabizadeh, H., Hajj, E.Y., Siddharthan, R.V., Nimeri, M., Elfass, S., and Piratheepan, M. (2019). *Analysis Procedures for Evaluating Superheavy Load Movement on Flexible Pavements, Volume V: Appendix D, Estimation of Subgrade Shear Strength Parameters Using Falling Weigh Deflectometer*, FHWA-HRT-18-053, Federal Highway Administration, Washington, DC.
6. Nabizadeh, H., Siddharthan, R.V., Elfass, S., and Hajj, E.Y. (2019). *Analysis Procedures for Evaluating Superheavy Load Movement on Flexible Pavements, Volume VII: Appendix F, Failure Analysis of Sloped Pavement Shoulders*, Report No. FHWA-HRT-18-055, Federal Highway Administration, Washington, DC.
7. Nabizadeh, H., Elfass, S., Hajj, E.Y., Siddharthan, R.V., Nimeri, M., and Piratheepan, M. (2019). *Analysis Procedures for Evaluating Superheavy Load Movement on Flexible Pavements, Volume VIII: Appendix G, Risk Analysis of Buried Utilities Under Superheavy Load Vehicle Movements*, Report No. FHWA-HRT-18-056, Federal Highway Administration, Washington, DC.
8. Batioja-Alvarez, D.D., Hajj, E.Y., and Siddharthan, R.V. (2018). *Analysis Procedures for Evaluating Superheavy Load Movement on Flexible Pavements, Volume IX: Appendix H, Analysis of Cost Allocation Associated with Pavement Damage Under a Superheavy Load Vehicle Movement*, Report No. FHWA-HRT-18-057, Federal Highway Administration, Washington, DC.

9. Kazemi, S.F., Nabizadeh, H., Nimeri, M., Batioja-Alvarez, D.D., Hajj, E.Y., Siddharthan, R.V., and Hand, A.J.T. (2018). *Analysis Procedures for Evaluating Superheavy Load Movement on Flexible Pavements, Volume X: Appendix I, Analysis Package for Superheavy Load Vehicle Movement on Flexible Pavement (SuperPACK)*, Report No. FHWA-HRT-18-058, Federal Highway Administration, Washington, DC.
10. Terzaghi, K. (1943). *Theoretical Soil Mechanics*, J. Wiley and Sons, Inc., New York, NY.
11. Das, B.M. (2010). *Principles of Foundation Engineering*, Seventh Edition, Cengage Learning, Boston, MA.
12. Meyerhof, G.G. (1953). "The Bearing Capacity of Foundations under Eccentric and Inclined Loads." *Proceedings of the Third International Conference on Soil Mechanics and Foundation Engineering, I*, pp. 440–445, Zürich, Switzerland.
13. Brinch Hansen, J. (1970). *A Revised and Extended Formula for Bearing Capacity*, Danish Geotechnical Institute, Lyngby, Denmark.
14. Vesić, A.S. (1973). "Analysis of ultimate loads of shallow foundations." *Journal of the Soil Mechanics and Foundations Division, 99*(1), pp. 45–73, American Society of Civil Engineers, Reston, VA.
15. Meyerhof, G.G. (1963). "Some Recent Research on the Bearing Capacity of Foundations." *Canadian Geotechnical Journal, 1*(1), pp. 16–26, Canadian Science Publishing, Ontario, Canada.
16. Prandtl, L. (1921). "Hauptaufsätze: Über die eindringungsfestigkeit (härte) plastischer baustoffe und die festigkeit von schneiden." *ZAMM-Journal of Applied Mathematics and Mechanics/Zeitschrift für Angewandte Mathematik und Mechanik, 1*(1), pp. 15–20, WILEY-VCH Verlag GmbH & Co. KGaA, Weinheim, Germany.
17. Reissner, H. (1924). "Zum Erddruckproblem." *Proceedings of the First International Congress of Applied Mechanics*, pp. 295–311, Delft, Netherlands.
18. Caquot, A. and Kerisel, J. (1953). "Sur le terme de surface dans le calcul des fondations en milieu pulverulent." *Proceedings of the Third International Conference on Soil Mechanics and Foundation Engineering, I*, pp. 336–337, Zürich, Switzerland.
19. De Beer, E.E. (1970). "Experimental Determination of the Shape Factors and Bearing Capacity Factors of Sand." *Geotechnique, 20*(4), pp. 387–411, ICE Publishing, Westminster, London, England.
20. Hanna, A.M. and Meyerhof, G.G. (1981). "Experimental Evaluation of Bearing Capacity of Footings Subjected to Inclined Loads." *Canadian Geotechnical Journal, 18*(4), pp. 599–603, Canadian Science Publishing, Ontario, Canada.

21. University of Nevada, Reno. (2013). *3D-Move Analysis Software*, V2.1, Reno, NV. Available online at: <http://www.arc.unr.edu/Software.html#3DMove>, last accessed September 19, 2017.
22. Siddharthan, R.V., Yao, J., and Sebaaly, P.E. (1998). "Pavement strain from moving dynamic 3D load distribution." *Journal of Transportation Engineering*, 124(6), pp. 557–566, American Society of Civil Engineers, Reston, VA.
23. Hajj, E.Y., Ulloa, A., Siddharthan, R., and Sebaaly, P.E. (2010). "Estimation of Stress Conditions for the Flow Number Simple Performance Test." *Transportation Research Record*, 2181, pp. 67–78, Transportation Research Board, Washington, DC.
24. Minnesota Department of Transportation. (2007). *MnDOT Pavement Design Manual*, Minnesota Department of Transportation, Saint Paul, MN.
25. Koloski, J., Schwarz, S., and Tubbs, D. (1989). "Geotechnical Properties of Geologic Materials." *Engineering Geology in Washington*, 1, Bulletin 78, Washington Division of Geology and Earth Resources, Olympia, WA.
26. Meyerhof, G.G. (1957). *The ultimate bearing capacity of foundations on slopes*, Technical Memorandum, Division of Building Research, National Research Council, Ottawa, Canada.
27. Saran, S., Sud, V.K., and Handa, S.C. (1989). "Bearing Capacity of Footings Adjacent to Slopes." *Journal of Geotechnical Engineering*, 115(4), pp. 553–573, American Society of Civil Engineers, Reston, VA.
28. Das, B.M. (2009). *Shallow Foundations Bearing Capacity and Settlement*, Second Edition, CRC Press, Boca Raton, FL.
29. Mizuno, T., Tokumitsu, Y., and Kawakami, H. (1960). "On the Bearing Capacity of a Slope of Cohesionless Soil." *Soils and Foundations*, 1(2), pp. 30–37, Japanese Geotechnical Society, Tokyo, Japan.
30. Chen, W.F. (2007). *Limit Analysis and Soil Plasticity*, J. Ross Publishing, Fort Lauderdale, FL.
31. Siva, R. and Mogaliah, G. (1975). "Bearing capacity of shallow foundations on slopes." *Indian Geotechnical Journal*, 5(4), pp. 237–253, Springer, Cham, Switzerland.
32. Drucker, D.C. and Prager, W. (1952). "Soil Mechanics and Plastic Analysis or Limit Design." *Quarterly of Applied Mathematics*, 10(2), pp. 157–165, Brown University, Providence, RI.
33. Nabizadeh, H., Hajj, E.Y., Siddharthan, R., Elfass, S., and Sebaaly, P.E. (2016). "Estimation of In-Situ Shear Strength Parameters for Subgrade Layer Using Non-destructive Testing." *The Roles of Accelerated Pavement Testing in Pavement Sustainability*, pp. 525–538, Springer, Cham, Switzerland.

34. Seyed-Farzan, K. (2018). *3D-FAST: Three-Dimensional Fourier Analysis of Pavement Structures Under Transient Loading*, Ph.D. Dissertation, Department of Civil and Environmental Engineering, University of Nevada, Reno, NV.
35. Chow, L.C., Mishra, D., and Tutumluer, E. (2014). “Framework for Development of an Improved Unbound Aggregate Base Rutting Model for Mechanistic–Empirical Pavement Design.” *Transportation Research Record*, 2401, pp. 11–21, Transportation Research Board, Washington, DC.
36. Kazmee, H. and Tutumluer, E. (2015). *Evaluation of Aggregate Subgrade Materials Used as Pavement Subgrade/Granular Subbase*, Report No. FHWA-ICT-15-013, Federal Highway Administration, Washington, DC.
37. Seyhan, U. and Tutumluer, E. (2002). “Anisotropic Modular Ratios as Unbound Aggregate Performance Indicators.” *Journal of Materials in Civil Engineering*, 14(5), pp. 409–416, American Society of Civil Engineers, Reston, VA.
38. Tutumluer, E., Kim, I.T., and Santoni, R.L. (2004). “Modulus Anisotropy and Shear Stability of Geofiber-Stabilized Sands.” *Transportation Research Record*, 1874, pp. 125–135, Transportation Research Board, Washington, DC.

